UNIVERSITY OF CRETE

MASTER THESIS

Autoionization Resonances strongly driven by Stochastic fields

Author:
George Mouloudakis

Supervisor:
Prof. Xenophon Zotos
Prof. Peter Lambropoulos

A thesis submitted in fulfillment of the requirements
for the degree of Master of Science

in the

Department of Physics

September 27, 2017

University of Crete

Abstract

Department of Physics

Master of Science

Autoionization Resonances strongly driven by Stochastic fields

by George Mouloudakis

The availability of strong, short pulse duration and high frequency (XUV and beyond) radiation through recent FEL sources opens up new prospects in the exploration of the strong driving of Autoionization (AI) resonances through photoabsorption experiments. However, such sources exhibit strong stochastic fluctuations leading to a finite bandwidth, that, until now, have not been considered in the theoretical literature of the excitation of AI resonances, simply because the traditional photoabsorption studies of AI states have been carried out mainly by means of weak, practically monochromatic synchrotron radiation sources. As shown in this thesis, a formulation of the problem including the effects of the stochastic character of the radiation fields reveals that under certain values of the relevant parameters the resulting AI profiles can be distorted dramatically and bear no resemblance to traditional Fano resonances.

Acknowledgements

I would like to thank my supervisors Prof. Xenophon Zotos and Prof. Peter Lambropoulos for their assistance and essential support they offered me all this years. Particularly the collaboration with Prof. Peter Lambropoulos, which started two years before, while I was still an undergraduate student, was really determinative and enlighting for me. I am grateful for the time that he spent all those years on teaching me essential theoretical tools that will be helpful for the rest of my academic life, but also for his guidance in the process of exploration of the wonderful world of quantum physics. I would also like to thank my brother Kostas Mouloudakis for all the enlightening discussions we had about physics in general, but also for our discussions relevant to the subject of this thesis.

Contents

List of Figures

Dedicated to my family

Chapter 1

Introduction

Autoionizing (AI) states, also referred to as resonances, in atoms and molecules belong to a rich field of Atomic Molecular and Optical (AMO) physics, representing a paradigm of discreet states embedded in continua. Typically, they can be excited either by photoabsorption or by collisions with electrons. The simplest case in point is represented by a so-called isolated AI resonance, which means that the width of its excitation profile is much smaller than the energy distance from the nearest AI resonance. A textbook example of an isolated resonance is provided by the doubly excited 2s2p state of Helium, which has been studied in exhaustive detail, both theoretically and experimentally, over the last 60 or so years [1].

Traditional photoabsorption studies of AI resonances have been carried out mainly by means of synchrotron radiation, where weak, practically monochromatic radiation excites the resonance. The observed quantity, as a function of the photon energy, can be either the amount of photoabsorption or photoelectron energy, as well as angular distribution, spectrum. The availability of strong radiation sources, such as lasers, motivated the exploration of the behavior of resonant transitions, driven by strong, pulsed and possibly non-monochromatic radiation. Over the last 35 years or so, a plethora of related studies have addressed issues such as AC Stark splitting in strongly driven bound states in double optical resonance, including the effect of field fluctuations [2, 3]. These studies were limited to the optical or near UV spectral region, in which sources of sufficient intensity were at the time available. The strong driving of AI states, such as the 2s2p in Helium, which requires radiation in the XUV range, were beyond the reach of those sources. Nevertheless, some initial theoretical exploration of the expected behavior of a strongly driven AI state, as well as the case of double resonance, involving the strong coupling of two AI states were published as early as 1981 [4] and revisited much later [5], when short wavelength Free Electron Lasers (FEL) began delivering strong radiation in the XUV and beyond. Extension of that work to triply excited hollow states followed a few years later [6–8]. To the best of our knowledge, there are two examples [9, 10] of experimental work providing some evidence of the strong coupling of two AI states.

We need to define the notion of strong coupling in AI states. A formulation of an AI state, particularly valid for an isolated resonance, involves the superposition of a discreet state and the continuum to which it is coupled via intra-atomic interaction. Diagonalization of the relevant part of the Hamiltonian leads to a modification of the position of the discreet part and a decay rate, referred to as AI width, as it corresponds to the width of the profile of the resonance. As discussed in detail in next sections, the dipole matrix element coupling a bound state to the discreet part of the AI resonance multiplied by the electric field amplitude, to within some coefficients, represents an effective Rabi frequency characterizing the strength of the coupling. Under traditional synchrotron radiation experiments, that Rabi frequency in much smaller than the AI width. That is what we shall call weak coupling, in which case

the interaction is describable in terms of a transition probability per unit time (rate), as given by Fermi's golden rule. The coupling is strong when the above condition is reversed, which means the Rabi frequency is larger than the AI width. When an EM field couples two AI states, as for example in refs.[4, 5, 11], the field is strong when the Rabi frequency between the two AI states is larger than the AI width of at least one of the resonances.

The availability of strong, short pulse duration, short wavelength (XUV and beyond) radiation through the recent Free Electron Laser (FEL) sources provides the opportunity to explore the behavior of strongly driven AI resonances. For a pulse of high peak intensity, the pulse duration enters as an important parameter paired to the intensity. Clearly, under any intensity, given sufficiently long time exposure of any system to the radiation, complete ionization will ensue. When the intensity is high, even a seemingly short pulse duration can cause significant ionization, to the extent of distorting the resonance profile. This effect was noted in the early paper by Lambropoulos and Zoller [4], referred to as "time saturation", has until now been of only academic interest. But as shown in this thesis, a dramatic manifestation of its role has now been observed.

In addition to the high intensity and short pulse duration, at least at the present time, FEL's exhibit strong intensity fluctuations [2]. This means that the radiation seen by the atom has a non-zero bandwidth, while the Rabi frequency undergoes stochastic fluctuations. The influence of the bandwidth has not been considered in the theoretical literature, until now, simply because AI resonances tend to be much broader than the bandwidths of synchrotron sources. Under FEL radiation, however, that is no longer the case, which requires a formulation that accounts for the stochastic fluctuations of the field. Depending on the strength of the coupling to the radiation, it may be that only the bandwidth is of importance. In the most general case of strong driving, in the sense defined above, accounting for the intensity fluctuations becomes imperative, as discussed in next sections.

This work was motivated by ongoing experimental investigations on the excitation of the 2s2p AI resonance of He under radiation by FLASH, the interpretation of which turned out to require a reformulation of the existing theoretical treatments. As demonstrated in the sections that follow, hitherto "academic" effects such as time broadening have been found to cause dramatic distortion of the profile. While the theory of an AI resonance driven strongly by a stochastic field, with intensity fluctuations, poses challenging problems not readily amenable to the theoretical tools developed for strongly driven transitions between bound states [2].

Chapter 2

Autoionizing States - Theoretical Review

Autoionization is a process by which an atom or a molecule in an excited state spontaneously emits one of its electrons due to its interaction with a continuum. The most common example of an autoionizing state (or autoionizing resonance) is a bound state which involves the excitation of two electrons with total energy larger than the one-electron ionization threshold. Such states are unstable and will eventually decay non-radiatevely due to their interaction with the continuum. After the decay of such a state, we end up with one electron in the ground state of the remaining ion and one electron ejected from the atom. Contrary to the usual case of exponentially decaying states resulting Lorentzian line-shapes, AIS line-shapes' are asymmetric. This asymmetry arises from the interference of the direct ionization path (from the ground state of the atom) and the ionization via the AIS due to its interaction with the continuum, usually referred as configuration interaction.

In this chapter we will present the basic theoretical tools that enable the study of AIS resonances as well as some basic results concerning their behaviour in presence of electromagnetic radiation.

2.1 Fano's Theoretical Treatment

The first theoretical study of autoionization resonances' lineshapes was held by Ugo Fano in 1935 [12], with a theory that describes the interference between an autoionizing state (AIS) and a continuum. This theory was not completed until 1961, where Fano extended his own theory by taking also into account the energy dependence of the AIS - continuum interaction [13]. Fano's work is time-independent and valid in the weak coupling limit where Rabi cycling and strong field phenomena do not take place. He begins by considering an interaction V between a discrete state $|\varphi\rangle$ and a non-degenerate set of states $|\psi_{\mathrm{E}}\rangle$. Due to this interaction, the Hamiltonian in the $|\varphi\rangle, |\psi_{\mathrm{E}}\rangle$ basis is no longer diagonal, with its matrix elements given by:

$$\begin{aligned} &\langle\varphi| H |\varphi\rangle = \mathrm{E}_{\varphi} \\ &\langle\psi_{\mathrm{E}'}| H |\varphi\rangle = V_{E'} \\ &\langle\psi_{\mathrm{E}'}| H |\psi_{\mathrm{E}''}\rangle = \mathrm{E}'\delta(\mathrm{E}'' - \mathrm{E}') \end{aligned} \tag{2.1}$$

where the ground state is assumed energetically far away from the AIS and is, for the moment, neglected .
The vector that diagonalises our Hamiltonian is expressed as

$$|\Psi_E\rangle = a_E |\varphi\rangle + \int dE' b_{E'} |\psi_{\mathrm{E}'}\rangle \tag{2.2}$$

thus the eigenvalue problem $H\left|\Phi_E\right\rangle = \mathrm{E}\left|\Phi_E\right\rangle$ leads to a set of coupled equations:

$$\begin{array}{l} \mathrm{E}_\varphi a_E + \int dE' V^*_{E'} b_{E'} = E a_E \\ V_{E'} a_E + E' b_{E'} = E b_{E'} \end{array} \tag{2.3}$$

that need to be solved in order to find the eigenvector of the new Hamiltonian. With proper algebraic manipulations, one can find that the formal solution of the second equation is

$$b_{E'} = \left[\frac{1}{E-E'} + z(E)\delta(E-E')\right] V_{E'} a_E \tag{2.4}$$

Now we can get the resulting expressions of the unknown coefficients:

$$a_E = \frac{\sin\Delta}{\pi V_E} \tag{2.5}$$

$$b_{E'} = \frac{V_{E'}}{\pi V_E}\frac{\sin\Delta}{E-E'} - \cos\Delta\delta(E-E') \tag{2.6}$$

where we defined

$$\Delta = -\arctan\frac{\pi|V_E|^2}{E-E_\varphi-F(E)} \tag{2.7}$$

The energy shift $F(E)$ is given by

$$F(E) = P\int dE' \frac{|V_{E'}|^2}{E-E'} \tag{2.8}$$

with P denoting the principal value part of the integral. Substituting (2.5) and (2.6) back to (2.2) , we find that the eigenvector of the Hamiltonian is

$$\begin{aligned} \left|\Psi_E\right\rangle &= \frac{\sin\Delta}{\pi V_E}\left|\varphi\right\rangle + P\int dE'\left[\frac{V_{E'}}{\pi V_E}\frac{\sin\Delta}{E-E'} - \cos\Delta\delta(E-E')\right]\left|\psi_{\mathrm{E}'}\right\rangle \\ &\equiv \frac{\sin\Delta}{\pi V_E}\left|\Phi\right\rangle - \cos\Delta\left|\psi_{\mathrm{E}}\right\rangle \end{aligned} \tag{2.9}$$

The probability of excitation may be represented in terms of an suitable operator T relevant to mechanism of the excitation. The probability would be proportional to the squared matrix element of this operator between the initial state and $\left|\Psi_{\mathrm{E}}\right\rangle$. In view of the above, this matrix element can be expressed as:

$$\left\langle\Psi_{\mathrm{E}}\right|T\left|i\right\rangle = \frac{1}{\pi V^*_E}\left\langle\Phi\right|T\left|i\right\rangle\sin\Delta - \left\langle\psi_E\right|T\left|i\right\rangle\cos\Delta \tag{2.10}$$

Since $\sin\Delta$ is an even function of $\mathrm{E}-\mathrm{E}_\varphi-F$ and $\cos\Delta$ an odd function of this variable, the contributions to $\left\langle\Phi\right|T\left|i\right\rangle$ and $\left\langle\psi_E\right|T\left|i\right\rangle$ are interfering with opposite phase on the two sides of the resonance. There is a value of Δ (call it Δ_0) where the transition probability vanishes, obeying

$$\tan\Delta_0 = \frac{\pi V^*_{E_0}\left\langle\psi_E\right|T\left|i\right\rangle}{\left\langle\Phi\right|T\left|i\right\rangle} \tag{2.11}$$

Inverting equation (2.11) one gets,

$$\frac{1}{\tan\Delta_0} = \frac{\left\langle\Phi\right|T\left|i\right\rangle}{\pi V^*_{E_0}\left\langle\psi_E\right|T\left|i\right\rangle} \equiv q \tag{2.12}$$

This equation defines the Fano asymmetry parameter q, which is a measure of the relative strength between the two interfering channels. Defining the dimensionless reduced energy variable

$$\varepsilon = \frac{E - \mathrm{E}_{\varphi} - F(E)}{\Gamma/2} \tag{2.13}$$

where $\Gamma = 2\pi|V_E|^2$ is the inverse lifetime of the AIS, we can express the ratio of the transitions probabilities $|\langle\Psi_E|\, T\, |i\rangle|^2$ and $|\langle\psi_E|\, T\, |i\rangle|^2$ as:

$$\frac{|\langle\Psi_E|\, T\, |i\rangle|^2}{|\langle\psi_E|\, T\, |i\rangle|^2} = \frac{(q+\varepsilon)^2}{1+\varepsilon^2} \tag{2.14}$$

The resonant part of the absorption cross section is proportional to the factor $\frac{(q+\varepsilon)^2}{1+\varepsilon^2}$, which is responsible for the asymmetric character of the line-shape, as seen in figure 1. Notice that for negative values of q the destructive interference takes place for positive values of ε and vice versa. For $q = 0$ the profile is symmetric while for $q \to \infty$ in the sense that $q \gg \varepsilon$, the resulting profile is Lorentzian.

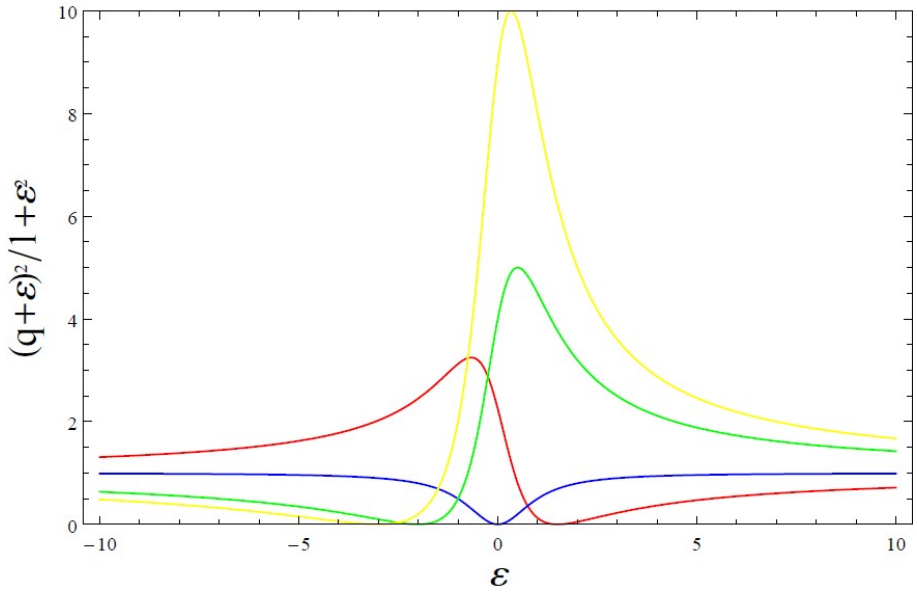

FIGURE 2.1: Fano's asymmetric line-shapes. Red Line: $q = -1.5$, Blue Line: $q = 0$, Green Line: $q = 2$, Yellow Line: $q = 3$

2.2 Basic Formulations

Although Fano's theory interprets successfully the asymmetric character of the AIS lineshapes, it is not directly applicable in the strong field limit. When the electromagnetic field that couples the ground state to the AIS becomes sufficiently large in the sense that the Rabi frequency becomes comparable to the AIS width, the transition can not be described necessarily in terms of a transition probability per unit time. In this case a treatment involving the calculation of the relevant matrix element between the ground state and the AIS is not adequate, and a dynamical approach has to be considered. The problem can be formulated in terms of the Schrödinger's

equation / Resolvent Formalism [4] or in terms of the density matrix [14, 15]. In this section we discuss all the possible theoretical treatments of the problem.

2.2.1 Schrödinger's equation

We begin by considering the eigenstates of the atomic part of the Hamiltonian H^0. The ground state is denoted by $|g\rangle$, the intermediate AIS by $|a\rangle$ and $|c\rangle$ is a set of continuum states. The energies of those states are denoted by E_g,E_a and E_c, respectively. The Hamiltonian of the compound system (atom + field) in a semi-classical approach can be expressed as $H = H^0 + V + D$, where D is the coupling to the radiation field and V the configuration interaction. It is often helpful to introduce the projection operators to the ground and the intermediate state, namely

$$P \equiv |g\rangle \langle g| \tag{2.15}$$

and

$$Q = |a\rangle \langle a| + \int dE_c \, |c\rangle \langle c| \tag{2.16}$$

respectively. The orthonormality of the eigenstates of the atomic part of the Hamiltonian reflects in the relations

$$P^2 = P \qquad PQ = 0 = QP \qquad Q^2 = Q \tag{2.17}$$

The two projection operators sum to unity in the approximation that assumes that other discrete states are energetically sufficiently far from $|a\rangle$ and can be neglected. The Hamiltonian in terms of the projection operators is written as:

$$H = (P+Q)H(P+Q) = PHP + PHQ + QHP + QHQ \tag{2.18}$$

The radiation field couples $|g\rangle$ to both $|a\rangle$ and $|c\rangle$, while $|a\rangle$ and $|c\rangle$ are coupled only via the configuration interaction. The matrix elements of the Hamiltonian in the basis of the eigenstates of H^0 are:

$$\langle a| H |a\rangle = \langle a| QHQ |a\rangle = \langle a| H^0 |a\rangle = E_a \tag{2.19}$$

$$\langle g| H |g\rangle = \langle g| PHP |g\rangle = \langle g| H^0 |g\rangle = E_g \tag{2.20}$$

$$\langle c| H |c'\rangle = \langle c| QHQ |c'\rangle = \langle c| H^0 |c'\rangle = E_c \delta(E_c - E_{c'}) \tag{2.21}$$

$$\langle c| H |a\rangle = \langle c| QHQ |a\rangle = \langle c| V |a\rangle \equiv V_{ca} \tag{2.22}$$

$$\langle a| H |g\rangle = \langle a| QHP |g\rangle = \langle a| D |g\rangle \equiv D_{ag} \tag{2.23}$$

$$\langle c| H |g\rangle = \langle c| QHP |g\rangle = \langle c| D |g\rangle \equiv D_{cg} \tag{2.24}$$

We are now ready to consider the time evolution of the system. We assume that at $t = 0$ the atom is in its ground state $|g\rangle$. At every time $t > 0$ the state of the system is expressed as:

$$|\Psi(t)\rangle = U_g(t) |g\rangle + \int d\tilde{E}' U_{\tilde{E}'}(t) |\Psi_{\tilde{E}'}\rangle \tag{2.25}$$

where according to the procedure leading to (2.9) $|\Psi_{\tilde{E}'}\rangle$ in our formulation is expressed as

$$|\Psi_{\tilde{E}'}\rangle = \frac{\sin \Delta(\tilde{E})}{\pi V_{\tilde{E}}} |\Phi_{\tilde{E}'}\rangle - \cos \Delta(\tilde{E}) |c\rangle \tag{2.26}$$

with

$$\left|\Phi_{\tilde{E}'}\right\rangle = |a\rangle + P\int dE_c \frac{V_{ca}(E_c)}{\tilde{E}-E_c}\,|c\rangle \tag{2.27}$$

$U_g(t)$ and $U_{\tilde{E}'}(t)$ are the corresponding time evolution operators of the states $|g\rangle$ and $\left|\Psi_{\tilde{E}'}\right\rangle$. The dynamical evolution of the wavefunction is determined by Schrödinger's equation, namely

$$i\hbar\tfrac{\partial}{\partial t}\,|\Psi(t)\rangle = H\,|\Psi(t)\rangle \qquad |\Psi(0)\rangle \;= |g\rangle \tag{2.28}$$

which upon substitution of (2.25) yields:

$$\frac{\partial}{\partial t}U_g(t)\,|g\rangle + \int d\tilde{E}'\frac{\partial}{\partial t}U_{\tilde{E}'}(t)\left|\Psi_{\tilde{E}'}\right\rangle = -\frac{i}{\hbar}HU_g(t)\,|g\rangle - \frac{i}{\hbar}\int d\tilde{E}'HU_{\tilde{E}'}(t)\left|\Psi_{\tilde{E}'}\right\rangle \tag{2.29}$$

We can now take the inner product of (2.29) with $\langle g|$ and $\left\langle\Psi_{\tilde{E}'}\right|$ separately, and obtain the following set of equations:

$$\frac{\partial}{\partial t}U_g(t) = -\frac{i}{\hbar}E_gU_g(t) - \frac{i}{\hbar}\int d\tilde{E}'\,\langle g|\,PHQ\left|\Psi_{\tilde{E}'}\right\rangle U_{\tilde{E}'}(t) \tag{2.30}$$

$$\frac{\partial}{\partial t}U_E(t) = -\frac{i}{\hbar}\tilde{E}'U_{\tilde{E}'}(t) - \frac{i}{\hbar}\left\langle\Psi_{\tilde{E}'}\right|QHP\,|g\rangle\,U_g(t) \tag{2.31}$$

with the initial conditions $U_g(0)=1$ and $U_{\tilde{E}'}(0)=0$. We will now introduce a new pair of coefficients defined as

$$u_g(t) \equiv U_g(t)e^{i\omega_g t} \qquad u_{\tilde{\omega}}(t) \equiv\; U_{\tilde{\omega}}(t)e^{i\tilde{\omega}t} \tag{2.32}$$

where $\omega_g \equiv E_g/\hbar$, $\tilde{\omega}\equiv\tilde{E}/\hbar$ and $U_{\tilde{\omega}}\equiv\hbar^{1/2}U_{\tilde{E}}$. Substitution of (2.32) back to (2.30) and (2.31) yields terms proportional to $e^{i[\omega\pm(\tilde{\omega}-\omega_g)]t}$. For ω tuned around the vicinity of the difference $\tilde{\omega}-\omega_g$, the exponent $e^{i[\omega+(\tilde{\omega}-\omega_g)]t}$ lead to terms that are anti-resonant with the photon frequency, while the opposite is true for the exponent $e^{i[\omega-(\tilde{\omega}-\omega_g)]t}$. For such frequencies the neglect of the anti-resonant terms stand as a very good approximation, also known as rotating wave approximation (RWA). The adoption of the RWA leads to the following set of equations:

$$\frac{\partial}{\partial t}u_g(t) = -i\int d\tilde{\omega}M^*_{\tilde{\omega}g}\varepsilon_0 e^{i[\omega-(\tilde{\omega}-\omega_g)]t}u_{\tilde{\omega}}(t) \tag{2.33}$$

$$\frac{\partial}{\partial t}u_{\tilde{\omega}}(t) = -iM_{\tilde{\omega}g}\varepsilon_0^* e^{-i[\omega-(\tilde{\omega}-\omega_g)]t}u_g(t) \tag{2.34}$$

where $M_{\tilde{\omega}g}\equiv\left\langle\Psi_{\tilde{E}}\right|\mu\,|g\rangle\,\hbar^{-1/2} = \hbar^{-1/2}(\frac{\tilde{\mu}_{\tilde{\mathrm{E}}g}}{V^*_{\tilde{E}}}sin\Delta - \mu_{cg}cos\Delta)$ and $\tilde{\mu}_{\tilde{\mathrm{E}}g}\equiv\left\langle\Phi_{\tilde{E}}\right|\mu\,|g\rangle$. By μ we denote the projection of the dipole operator of the atom to the polarization vector of the radiation and by ε_0, the amplitude of the electric field $\mathrm{E}(t)=\varepsilon_0e^{i\omega t}+\varepsilon_0^*e^{-i\omega t}$. We have also used the fact the radiation interaction is written as $D=\vec{\mu}\cdot\vec{\varepsilon}E(t)$ where $\vec{\varepsilon}$ is the polarization vector of the external electric field. We note that the integration over all $\tilde{\omega}$ involved in (2.33) does not dispute the validity of the RWA due to the peaked nature of $M_{\tilde{\omega}g}$ seen as a function of $\tilde{\omega}$.

The solution of the system of equations (2.33) and (2.34) leads to the expressions for $u_g(t)$ and $u_{\tilde{\omega}}(t)$ and therefore, eventually, for $U_g(t)$ and $U_{\tilde{\omega}}(t)$. The time evolution of operator of the intermediate state is connected to $U_{\tilde{\omega}}(t)$ via

$$U_a(t) = \hbar^{-1/2}\int d\tilde{\omega}\frac{U_{\tilde{\omega}}(t)\sin\Delta}{\pi V_{\tilde{E}}} \tag{2.35}$$

according to the the relations (2.26) and (2.27). Finding the expressions for $U_g(t)$ and $U_a(t)$, one can form the quantity

$$P(t) = 1 - |U_g(t)|^2 - |U_a(t)|^2 \tag{2.36}$$

which is the probability of ionization at every time. We are usually concerned with calculating the ionization probability at a time after the atom-field interaction time, denoted by T. An equivalent expression for the ionization probability can be given by an integration over the whole continuum:

$$P(t) = \int dE_c |U_c(t)|^2 \tag{2.37}$$

We have to notice that in time T, some population would be in state $|a\rangle$. Since the rate of autoionization is much bigger than the spontaneous decay rate, this population will decay, non-radiatevely, into the continuum via the interaction V. To account for this population, the proper expression of the ionization probability at a time $t > T$ should be

$$P(t > T) = 1 - |U_g(T)|^2 - |U_a(T)|^2 e^{-\Gamma(t-\mathrm{T})} \tag{2.38}$$

In the long-time limit $\Gamma(t - T) \gg 1$, the ionization probability can be simplified to

$$P(t > T) = 1 - |U_g(T)|^2 \tag{2.39}$$

2.2.2 Resolvent Operator Formalism

In order to have a complete overview of the different theoretical treatments we can use to formulate our problem, we will now present the formulation in terms of the resolvent operator [4] which is equivalent to the Schrödinger's equation formalism. This time, we will treat the radiation field quantum mechanically, therefore the Hamiltonian would be $H = H^0 + V + D$, with H^0 containing an atomic part H^A and a radiation part H^R, i.e. $H^0 = H^A + H^R$. The eigenstates of the radiation part are the well-known photon-number states $|n\rangle$, while the eigenstates of the atomic part were defined in the previous subsection. The eigenstates of the compound system (atom + radiation) are tensor products of the above eigenstates. The initial state state of the system is $|g; n\rangle$ which is connected to $|\alpha; n-1\rangle$ via the absorption/emission of one photon. The initial state is also coupled to $|c; n-1\rangle$ via the same mechanism. Also a transition from $|\alpha; n-1\rangle$ to $|c; n-1\rangle$ can take place due to the presence of the configuration interaction V; therefore it is a non-radiative transition.

Since we treat the radiation field quantum mechanically, the Hamiltonian is time dependent and the time evolution of the wavefunction is given by

$$|\Psi(t)\rangle = e^{-iHt/\hbar} |\Psi(0)\rangle \equiv U(t) |\Psi(0)\rangle \tag{2.40}$$

We now define the resolvent operator $G(z)$ according to:

$$G(z) \equiv \frac{1}{z - H} = \frac{1}{z - H^0 - V - D} \tag{2.41}$$

that is related to the time evolution operator via

$$U(t) = -\frac{1}{2\pi i}\int_{-\infty}^{+\infty} dx e^{-ixt} G^{+}(x) \tag{2.42}$$

with $G^{+}(x) = \lim_{\eta\to 0^{+}} G(x+i\eta)$. The wavefunction of the system at every time $t > 0$ is given by

$$|\Psi(t)\rangle = U_{gg}(t)\,|g;n\rangle + U_{ag}(t)\,|\alpha;n-1\rangle + \int dE_c U_{cg}\,|c;n-1\rangle \tag{2.43}$$

If the relevant matrix elements of the resolvent operator are found, then we can find the matrix elements of the time evolution operator via (2.42) and the problem is solved. The Resolvent operator satisfies the equation

$$(z-H)G = 1 \Leftrightarrow (z-H)(P+Q)GP = P \tag{2.44}$$

We multiply (2.44) two times from the left, one with P and one with Q and use the properties of the projection operators to obtain the set:

$$(z-PHP)(PGP) - (PHQ)(QGP) = P \tag{2.45}$$

$$(z-QHQ)(QGP) - (QHP)(PGP) = 0 \tag{2.46}$$

Taking inner products of (2.45) and (2.46) with the atomic eigenstates one can easily find

$$(z-E'_g)G_{gg} - D_{ga}G_{ag} - \int dE'_c D_{gc}G_{cg} = 1 \tag{2.47}$$

$$-D_{ag}G_{gg} + (z-E'_a)G_{ag} - \int dE'_c V_{ac}G_{cg} = 0 \tag{2.48}$$

$$-D_{cg}G_{gg} - V_{ca}G_{ag} + (z-E'_c)G_{cg} = 0 \tag{2.49}$$

where we used the relations $G_{gg} = \langle g|\,PGP\,|g\rangle$, $G_{ag} = \langle a|\,QGP\,|g\rangle$ and $G_{cg} = \langle c|\,QGP\,|g\rangle$. The energies E'_i, $i = g, a, c$ contain the atomic energies and an energy $\hbar\omega$ multiplied by the number of photons that occupy the relevant mode. Solving (2.49) for G_{cg}, one gets

$$G_{cg} = \frac{1}{z-E'_c}(D_{cg}G_{gg} + V_{ca}G_{ag}) \tag{2.50}$$

The substitution of (2.50) to (2.47) and (2.48) leads to a coupled system of G_{gg} and G_{ag}, whose solution is

$$G_{gg} = 1/\Lambda(z) \tag{2.51}$$

$$G_{\alpha g} = \frac{D_{ag} + \int dE'_c \frac{V_{ac}D_{cg}}{z-E'_c}}{(z-E'_a - \int dE'_c \frac{|V_{ac}|^2}{z-E'_c})\Lambda(z)} \tag{2.52}$$

where

$$\Lambda(z) = z - E'_g - \int dE'_c \frac{|D_{cg}|^2}{z-E'_c} - \frac{(D_{ga} + \int dE'_c \frac{D_{gc}V_{ca}}{z-E'_c})(D_{ag} + \int dE'_c \frac{V_{ac}D_{cg}}{z-E'_c})}{z-E'_a - \int dE'_c \frac{|V_{ac}|^2}{z-E'_c}} \tag{2.53}$$

Assuming that the matrix elements involved in the integrals over E'_c are slowly

varying functions of E'_c in the vicinity of the resonance, we can replace z by $E'_g + i\varepsilon$, with $\varepsilon \to 0^+$. Using the formula $\frac{1}{x-x_0+i\varepsilon} = P\frac{1}{x-x_0} - i\pi\delta(x-x_0)$, we get

$$\frac{1}{z - {E'}_c} = \lim_{\varepsilon\to 0^+} \frac{1}{{E'}_g - {E'}_c + i\varepsilon} = P\int \frac{d{E'}_c}{{E'}_g - {E'}_c} - i\pi\delta({E'}_g - {E'}_c) \tag{2.54}$$

The substitution of (2.54) back to the integrals leads to the following shifts and widths:

$$\int d{E'}_c \frac{|D_{cg}|^2}{z - {E'}_c} \simeq P\int d{E'}_c \frac{|D_{cg}|^2}{{E'}_g - {E'}_c} - i\pi\left|D_{cg}({E'}_g)\right|^2 \equiv S_g - i\frac{1}{2}\gamma_g \tag{2.55}$$

$$\int d{E'}_c \frac{|V_{ca}|^2}{z - {E'}_c} \simeq P\int d{E'}_c \frac{|V_{ca}|^2}{{E'}_g - {E'}_c} - i\pi\left|V_{ca}({E'}_g)\right|^2 \equiv F_a - i\frac{1}{2}\Gamma_\alpha \tag{2.56}$$

The quantities S_g and F_a represent the shifts of the states $|g\rangle$ and $|\alpha\rangle$, respectively while γ_g is the ionization width of the ground state due to its direct coupling to the continuum and Γ_α is the AIS width. From the solution of the system of equations (2.51) and (2.52), we can find the expressions for $U_{gg}(t)$ and $U_{ag}(t)$ and form the ionization probability at times $t > T$ as before:

$$P(t > T) = 1 - |U_{gg}(T)|^2 - |U_{ag}(T)|^2 e^{-\Gamma_a(t-T)} \tag{2.57}$$

2.2.3 Density Matrix Formulation

In this subsection we will present the treatment of the problem in terms of the density matrix [14, 15]. The formulation in terms of the density matrix is the suitable formulation in order to deal with cases where the external field undergoes stochastic fluctuations, a case where the Schrödinger's equation formalism is not directly applicable. This particular case is studied with exclusive detail in following chapters.

We slightly change the notation introduced in the previous subsection and denote the ground state with $|1\rangle$ and the AIS state with $|2\rangle$. Our total Hamiltonian is still the same as defined above, i.e. $H = H^0 + V + D$. The equation of motion of the density operator is

$$i\hbar\dot{\rho} = \Big[H^0 + D + V, \rho\Big] \tag{2.58}$$

from which we obtain the set of equations that determine the time evolution of its matrix elements:

$$\dot{\rho}_{11} = -i\hbar^{-1}\left(D_{12}\rho_{21} + \sum_c D_{1c}\rho_{c1} - c.c.\right) \tag{2.59}$$

$$\dot{\rho}_{22} = -i\hbar^{-1}\left(D_{21}\rho_{12} + \sum_c V_{2c}\rho_{c2} - c.c.\right) \tag{2.60}$$

$$\dot{\rho}_{21} = -i\omega_{21}\rho_{21} - i\hbar^{-1}\left(D_{21}\rho_{11} + \sum_c V_{2c}\rho_{c1} - \rho_{22}D_{21} - \sum_c \rho_{2c}D_{c1}\right) \tag{2.61}$$

$$\dot{\rho}_{c1} = -i\omega_{c1}\rho_{c1} - i\hbar^{-1}\left(D_{c1}\rho_{11} + \sum_c V_{c2}\rho_{21} - \sum_c \rho_{c2}D_{21}\right) \tag{2.62}$$

$$\dot{\rho}_{c2} = -i\omega_{c2}\rho_{c2} - i\hbar^{-1}\left(D_{c1}\rho_{12} + \sum_c V_{c2}\rho_{22} - \sum_c \rho_{c1}D_{12}\right) \tag{2.63}$$

where the summations $\sum_c$ are over all virtual states and $\omega_{ij} \equiv \omega_i - \omega_j$.

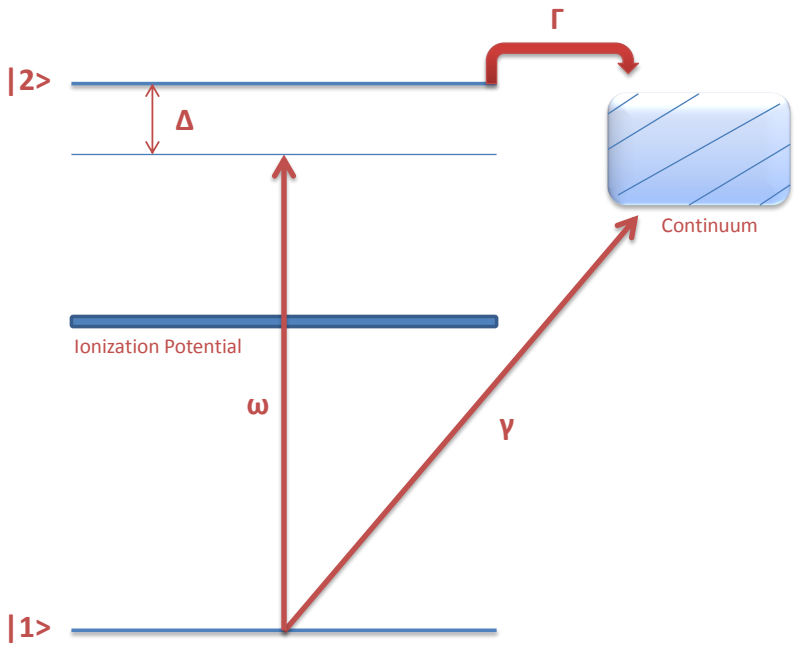

FIGURE 2.2: Density Matrix Formulation - Energy levels Diagram

The single dipole matrix elements can be expressed as a product of the dipole moment and the electric field amplitude, namely $D_{ij} = \mu_{ij}\mathcal{E}(t)$. The electric field is defined as $E = \mathcal{E}(t)e^{i\omega t} + c.c.$ We now introduce a new set of slowly varying amplitudes σ_{ij}, satisfying the relations $\rho_{ii} = \sigma_{ii}$ $(i = 1, 2)$, $\rho_{21} = \sigma_{21}e^{-i\omega t}$, $\rho_{c1} = \sigma_{c1}e^{-i\omega t}$ and $\rho_{c2} = \sigma_{c2}$. Under the adoption of the Rotating Wave Approximation the set of equations (2.59) to (2.63) for the new variables become:

$$\dot{\sigma}_{11} = -i\hbar^{-1}\left(\mu_{12}\mathcal{E}(t)\sigma_{21} + \sum_c \mu_{1c}\mathcal{E}(\mathrm{t})\sigma_{c1} - c.c.\right) \tag{2.64}$$

$$\dot{\sigma}_{22} = -i\hbar^{-1}\left(\mu_{21}\mathcal{E}^*(t)\sigma_{12} + \sum_c V_{2c}\sigma_{c2} - c.c.\right) \tag{2.65}$$

$$\dot{\sigma}_{21} = i(\omega - \omega_{21})\sigma_{21} - i\hbar^{-1}\left[\mu_{21}\mathcal{E}(\mathrm{t})(\sigma_{11} - \sigma_{22}) + \sum_c V_{2c}\sigma_{c1} - \sum_c \mu_{c1}\mathcal{E}(t)\sigma_{2c}\right] \tag{2.66}$$

$$\dot{\sigma}_{c1} = i(\omega - \omega_{c1})\sigma_{c1} - i\hbar^{-1}\left(\mu_{c1}\mathcal{E}^*(t)\sigma_{11} + V_{c2}\sigma_{21} - \mu_{21}\mathcal{E}^*(t)\sigma_{c2}\right) \tag{2.67}$$

$$\dot{\sigma}_{c2} = -i\omega_{c2}\sigma_{c2} - i\hbar^{-1}\left(\mu_{c1}\mathcal{E}^{*}(t)\sigma_{12} + V_{c2}\sigma_{22} - \mu_{12}\mathcal{E}(\mathrm{t})\sigma_{c1}\right) \tag{2.68}$$

In the last two equations we can apply the adiabatic approximation and set the time derivatives equal to zero. After solving the resulting system for σ_{c1} and σ_{c2} we find:

$$\sigma_{c1} \simeq \frac{1}{\hbar(\omega - \omega_{c1}) + i\varepsilon}\left(\mu_{c1}\mathcal{E}(t)\sigma_{11} + V_{c2}\sigma_{21}\right) \tag{2.69}$$

$$\sigma_{c2} \simeq \frac{-1}{\hbar\omega_{c2} - i\varepsilon}\left(\mu_{c1}\mathcal{E}^{*}(t)\sigma_{12} + V_{c2}\sigma_{22}\right) \tag{2.70}$$

where we introduced ε as a very small positive number. Substituting (2.69) back to (2.64) one gets

$$\dot{\sigma}_{11} = 2\hbar^{-1}\mathrm{Im}\left[\sum_{c}\frac{\left|\mu_{1c}\mathcal{E}(\mathrm{t})\right|^{2}}{\hbar(\omega - \omega_{c1})}\sigma_{11}\right] + 2\hbar^{-1}\mathrm{Im}\left[\mu_{12}\mathcal{E}(t) + \sum_{c}\frac{\mu_{1c}\mathcal{E}(\mathrm{t})V_{c2}}{\hbar(\omega - \omega_{c1})}\sigma_{21}\right] \tag{2.71}$$

We now define the following quantities:

$$\Omega(t) \equiv \frac{\mu_{12}\mathcal{E}(\mathrm{t})}{\hbar} + P\sum_{c}\frac{\mu_{1c}\mathcal{E}(t)V_{c2}}{\hbar^{2}(\omega - \omega_{c1})} \tag{2.72}$$

$$q \equiv \frac{\Omega(t)}{\pi\hbar^{-2}\left(\mu_{1c}\mathcal{E}(\mathrm{t})V_{c2}\right)_{\omega_c = \omega_1 + \omega}} \tag{2.73}$$

$$S_1 - \frac{i}{2}\gamma(t) \equiv \hbar^{-2}\sum_{c}\frac{\left|\mu_{1c}\mathcal{E}(\mathrm{t})\right|^{2}}{\omega - \omega_{c1} + i\varepsilon} \tag{2.74}$$

that represent the Rabi frequency of the driving $|1\rangle \leftrightarrow |2\rangle$, the asymmetry parameter introduced in previous subsections, the Stark shift of the ground state and the rate of the direct transition to the continuum, respectively. In view of the above, equation (2.71) can be written in the form:

$$\partial_t\sigma_{11}(t) = -\gamma(t)\sigma_{11}(t) + 2Im\left\{\Omega(t)\left(1 - \frac{i}{q}\right)\sigma_{21}(t)\right\} \tag{2.75}$$

Following the same procedure, we can bring the equation that governs the time evolution of $\sigma_{22}(t)$, in the form

$$\partial_t\sigma_{22}(t) = -\Gamma\sigma_{22}(t) - 2Im\left\{\Omega(t)\left(1 + \frac{i}{q}\right)\sigma_{21}(t)\right\} \tag{2.76}$$

where we introduced the definition

$$S_2 - \frac{i}{2}\Gamma \equiv \hbar^{-2}\sum_{c}\frac{\left|V_{c2}\right|^{2}}{\omega - \omega_{c1} + i\varepsilon} \tag{2.77}$$

reflecting the Stark shift of state $|2\rangle$ and its non-radiative decay to continuum via the configuration interaction, respectively. Finally, the time evolution of the off-diagonal matrix element σ_{21} is determined by

$$\left[\partial_t - i\Delta + \frac{1}{2}\left(\gamma(t) + \Gamma\right)\right]\sigma_{21}(t) = -i\Omega(t)\left(1 - \frac{i}{q}\right)\sigma_{11}(t) + i\Omega(t)\left(1 + \frac{i}{q}\right)\sigma_{22}(t) \tag{2.78}$$

where $\Delta \equiv \omega - [(\omega_2 + S_2) - (\omega_1 + S_1)]$. An inspection of the system of equations (2.75), (2.76) and (2.78) reveals that the system is driven by a generalized complex

Rabi frequency $\tilde{\Omega}(t) \equiv \Omega(t)\left(1 - \frac{i}{q}\right)$ that contains the asymmetry parameter q. Again, the ionization yield at a time $t > T$ is given by:

$$P(t) = 1 - \sigma_{11}(T) - \sigma_{22}(T)e^{-\Gamma(t-T)} \tag{2.79}$$

An interesting result arises in the case of weak driving, where the photoionization profile is expressed in terms of transition rate. We will show that this rate is proportional to the Fano factor (2.14). The weak driving implies the relations $\sigma_{11}(t) \approx 1$, $\sigma_{22}(t) \approx 0$ and $\dot{\sigma}_{21}(t) \approx 0$, therefore equation (2.78) becomes:

$$\sigma_{21} = \frac{-i}{-i\Delta + (\gamma + \Gamma)/2}\Omega\left(1 - \frac{i}{q}\right) \tag{2.80}$$

Substitution of equation (2.79) back to (2.75), leads to the following rate:

$$\dot{\sigma}_{11} = -\gamma - \frac{1}{1+\varepsilon^2}\left\{\frac{\Omega^2}{q^2\Gamma/2}(q+\varepsilon)^2 - (\varepsilon^2+1)\frac{\Omega^2}{q^2\Gamma/2}\right\} \tag{2.81}$$

where we defined the dimensionless detuning $\varepsilon \equiv \frac{\Delta}{(\Gamma/2)}$. It is important to note that the quantities γ, Γ, Ω and q are always related via the expression $4\Omega^2 = q^2\gamma\Gamma$. After some algebraic manipulations of (2.80), it is straightforward to show that the photoionization rate, which is the rate of depopulation of state $|1\rangle$ (Fermi's Golden Rule), is expressed as:

$$R = -\dot{\sigma}_{11} \propto \frac{(q+\varepsilon)^2}{\varepsilon^2+1}\frac{\Omega^2}{q^2\Gamma/2} \tag{2.82}$$

Therefore the photoionization lineshape in the weak field limit follows the typical Fano profile.

2.3 Basic Results

In this section we will make a brief review of the basic results of the study of AIS driven by electromagnetic fields.

As we discussed earlier, although Fano's treatment provide a good understanding of the behaviour of AIS under Electromagnetic radiation and the arise of the asymmetric profile, it is only valid within the weak coupling limit. The first leap from Fano's weak field theory to a complete time dependent approach, that is valid irrelevant of the strength of the coupling, was held by P. Lambropoulos and P. Zoller in 1981 [4]. The theory was cast in terms of Schrodinger's equation / Resolvent Operator (see previous section) and included both the cases of a single (isolated) AI resonance and the coupling between two AIS.

In figure 2.3 they show the effects of the time of interaction T to the AI lineshape for a medium intensity field ($\Omega = \Gamma$). As long as the interaction time is sufficiently larger than the inverse AI lifetime, the typical asymmetric AI profile arises. However for small interaction times (in the order of the AI lifetime) the atom is not exposed to radiation sufficiently enough time for ionization to occur, therefore the profile is almost flat.

In the strong field limit the situation changes dramatically. The effects of the strong field coupling to an AI profile become evident in figure 2.4 where AI lineshapes are shown as function of the Rabi frequency, for an interaction time $T = 5\Gamma^{-1}$.

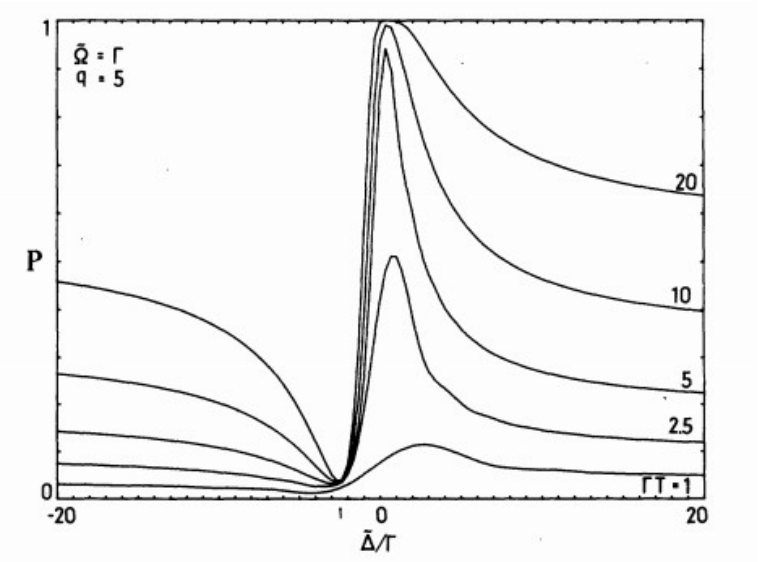

FIGURE 2.3: Line shape of an AI resonance as a function of the dynamical detuning, for various times of interaction. [4]

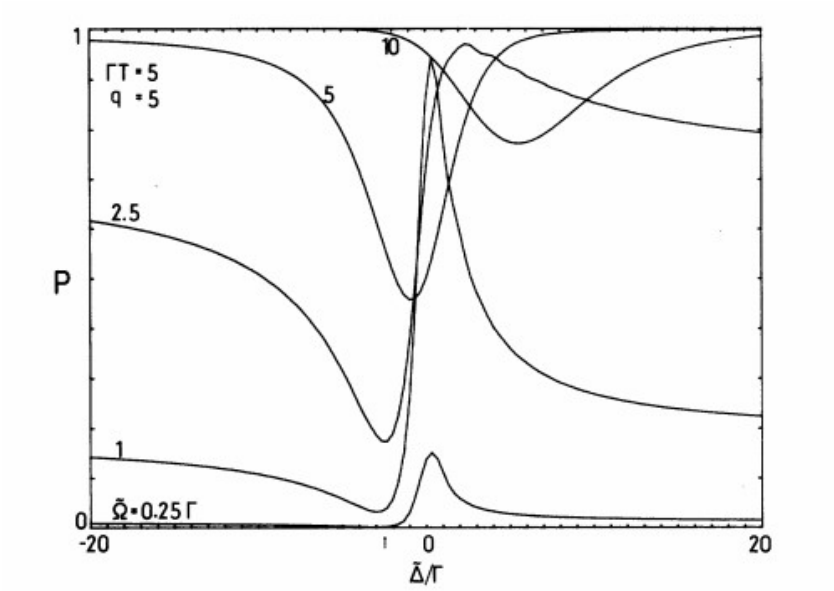

FIGURE 2.4: Line shape of an AI resonance as a function of the dynamical detuning, for various intensities. [4]

For medium intensities the typical profile is still clear. As the intensity increases the ionization tends to become unity, irrelevant of the value of the dynamical detuning and as a consequence the maximum no longer exists. The probability of ionization changes slower in the region around the minimum, but the minimum also tends to approach unity. The position of the minimum is also altered due to the intensity dependence of the transition amplitudes that interfere destructively to give rise to this minimum, therefore this effect should not be regarded as a Stark shift effect. For smaller interaction times ionization also occurs if the intensity is sufficient large.

Also, under any intensity the exposure of the atom to the radiation field for sufficiently long time will ensue ionization. In view of the above, it was concluded that it is the interplay between pulse duration and intensity that determines the shape of the profile, an effect that was referred as "time saturation". As we will see in next chapters this effect plays very important role in the determination of the profile of AI states under stochastic Electromagnetic fields.

The results of the AC Stark splitting [4, 5, 11] due to strong driving between two AIS are even more striking. A set of two AIS were chosen such that the first of them is sufficiently narrower than the second and can be regarded approximately as a bound state. The ground state is coupled to the first AIS via a weak transition, while a second field of varying intensity couples the two AIS. The second field is chosen such that its frequency is resonant with the respective transition (Notice that the term resonant implies the relation $\Delta = 0$ and in the figure the ionization probability is plotted as a function of the dynamical detuning in units of Γ). While the intensity of the second field increases we clearly begin to see the AC Stark splitting occurring. But contrary to the case of typical AC Stark splitting in double optical resonance between two bound states, the two peaks are unequal both in height and width. These new effect are due to the interference between the direct ionization and the ionization via the second state. One striking result is that as the intensity increases, one of the peaks tends to become narrower while the other tends to broaden. The interference can even cause the complete disappearance of one of the two peaks.

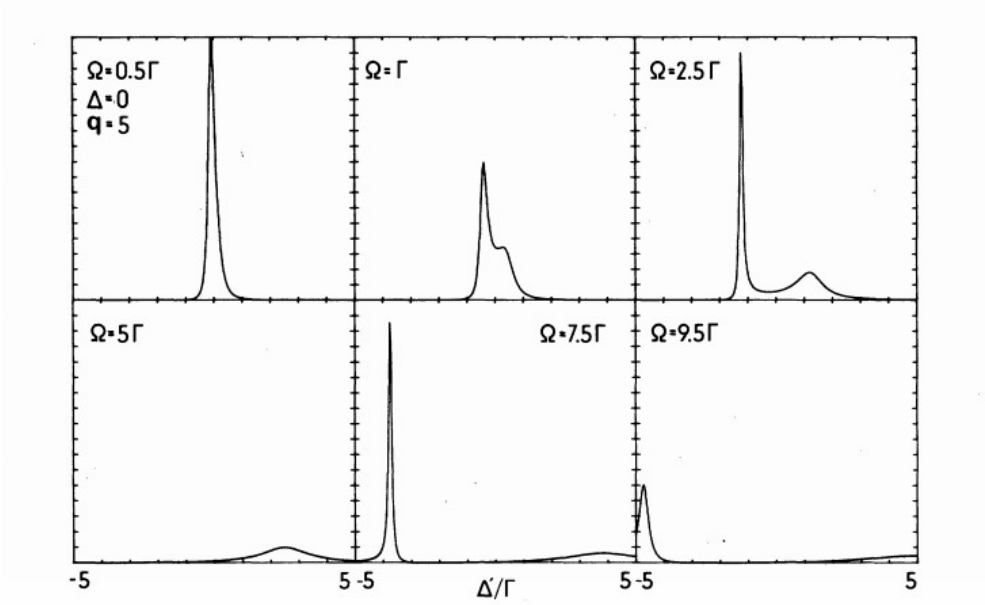

FIGURE 2.5: AC Stark Splitting of two strongly coupled AIS exactly on resonance $\Delta = 0$. Notice than in x-axis the detuning is dynamical (intensity dependant). [4]

Altough AC Stark splitting between two Autoionizing states has also been explored theoretically through the years with various formulations, the experimental investigation of that aspect has up to now been rather limited [9, 10].

The study of the effects of the phase of an electromagnetic field driving an AI resonance has also shown that its lineshape can be modified significantly [14, 15]. More specifically the theory was cast using a formulation in terms of the density matrix operator, using an electric field that couples the ground state to the AIS via

a one- and a three-photon transition. The relative phase of these transitions, which is controllable, leads to profound alternation of the ionization profile. One of the interesting results of the above study in the weak field limit is that the ionization rate can be written in the compact form:

$$P = \frac{2}{\varepsilon^2+1}\left|\frac{\Omega^{(3)}}{q^{(3)}(\Gamma/2)^{1/2}}(q^{(3)}+\varepsilon) + e^{i\varphi}\frac{\Omega}{q(\Gamma/2)^{1/2}}(q+\varepsilon)\right|^2 \tag{2.83}$$

where $\Omega^{(3)}$ is the effective three-photon Rabi frequency and $q^{(3)}$ the asymmetry parameter characterizing the three-photon transition. The relative phase between the two transitions is denoted by φ and ε is the normalized detuning defined as $\varepsilon \equiv \frac{\Delta}{(\Gamma/2)}$. Equation (2.83) reveals that if specific combinations of the coupling strengths and the relative phase are chosen, one can achieve complete cancellation of the direct transition to the continuum (resulting a Lorentzian lineshape) or complete cancellation of the transition to the discrete part, leaving only the direct transition (resulting a flat lineshape with a window at $\varepsilon = 0$). Some of these results are illustrated in figure 2.6.

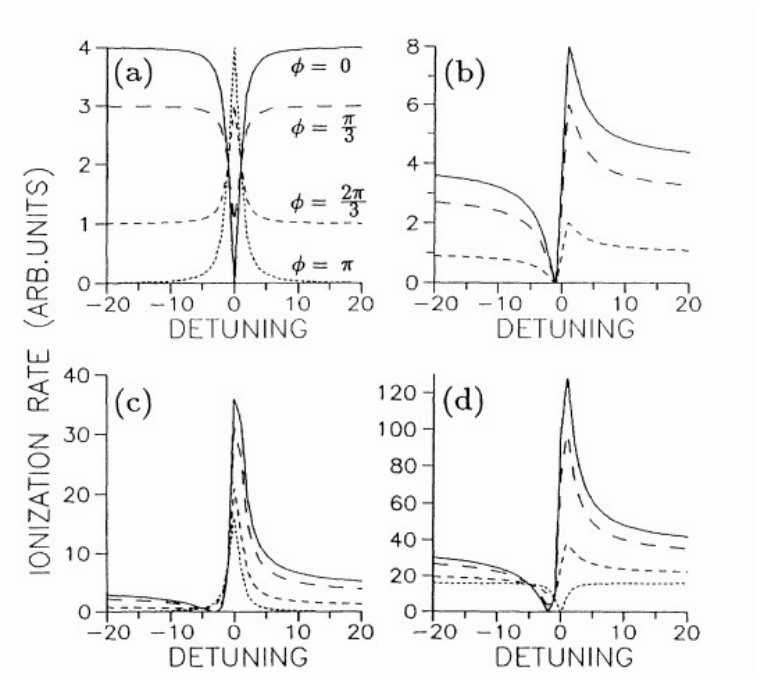

FIGURE 2.6: Effects of the relative phase between a one- and a three-photon transition to the autoionization lineshape in the weak field limit [15]. (a) $\Omega^{(3)} = 1$, $q^{(3)} = 1$, $\Omega = 1$, $q = -1$. (b) $\Omega^{(3)} = 1$, $q^{(3)} = 1$, $\Omega = 1$, $q = 1$. (c) $\Omega^{(3)} = 1$, $q^{(3)} = 5$, $\Omega = 1$, $q = 1$. (d) $\Omega^{(3)} = 1$, $q^{(3)} = 5$, $\Omega = 5$, $q = 1$.

The regime of strong intensities was also explored, where both the one- and three- photon Rabi frequencies are larger the the AI lifetime. In this case the ionization is not necessarily describable in terms of a rate and therefore a complete time-dependent calculation is inevitable. In figure 2.7 we can see that for low intensities, the profile is the typical Fano-like profile except for the extreme case of $\varphi = \pi$ where the resulting profile is symmetrical. As the intensity increases the profile is

modified significantly until it becomes completely flat, with a small window at $\varepsilon = 0$ in the strong field limit.

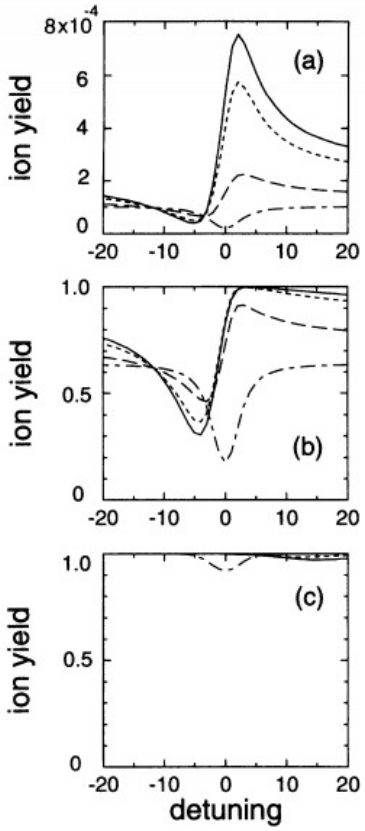

FIGURE 2.7: Effects of the relative phase between a one- and a three-photon transition to the autoionization lineshape in the weak to strong field limit [14]. For all graphs the chosen parameters are $q^{(3)} = 1$, $q = 1$, $\Gamma = 5$ and $= 2$. Solid line: $\varphi = 0$, Dotted line: $\varphi = \pi/3$, Dashed line: $\varphi = 2\pi/3$, Dot-dashed line: $\varphi = \pi$ (a) $\Omega^{(3)} = 0.01$, $\Omega = 0.01$ (b) $\Omega^{(3)} = 1$, $\Omega = 1$ (c) $\Omega^{(3)} = 5$, $\Omega = 5$.

Studies have also been carried out relevant to problem of the influence of autoionization structures on the single and double ionization signals, particularly for the Helium atom, where the relevant cross section of the ionization of the $He(1s)^+$ ions is of the order of the ionization of the neutral atom [16]. In this case the radiation can ionize the ions via the absorption of one additional photon, and this process can possibly be influenced by the presence of neighbouring AIS, just like $|2s2p\rangle$ and $|2s3p\rangle$. The results of this study revealed that the presence of such neighbouring states does not have any influence on the double ionization yield, however it can lead to an increase of the double to single ionization ratio especially for pulses of long duration.

Chapter 3

Stochastic Electromagnetic Fields

Most of the experiments that explore aspects of the interaction of electromagnetic fields with atoms, are interpreted with theories that do not account for the stochastic properties of the radiation fields. This is due to the fact that many of the radiation sources used in experiments have small bandwidths and can be indeed assumed monochromatic and purely coherent in some degree. For example, traditional photoabsorption experiments on AI resonances have been carried out mainly with synchrotron radiation sources, where the field is weak and approximately monochromatic. However, there are sources whose stochastic properties play significant role and can not be neglected. Theories that do not account for these properties can lead to false interpretations of such experiments, therefore the general background of how we treat for these properties seem to be of very importance.

3.1 General Description

In this section we will present the basic features of stochastically fluctuating electromagnetic fields and the tools that enable us to account for these features theoretically. Our ultimate goal is to apply some of these tools in the context of AI states to develop a theory that is general and accounts for all properties that, as we will discuss in the next section, seem to play more significant role on the determination of AI profiles than one could expect.

The problem is cast in terms of a atomic density matrix operator coupled to a stochastically fluctuating field of amplitude $\mathcal{E}(t)$ [2]. The stochastic character of the field leads to equations of motion which are also stochastic. Therefore these equations have to averaged over the field fluctuations. The averaging process for a N-photon transition leads to atomic-field correlations of the type $\left\langle \mathcal{E}^{*N}(t_1)\mathcal{E}^{N}(t_2)\rho_{ii}(t_2)\right\rangle$, that can not be generally evaluated without first solving the stochastic differential equations for the density matrix. Note that the angular brackets denote the averaging over the field fluctuations. As an approximation valid under certain conditions, one could decorrelate the atomic-field dynamics [17] by taking $\left\langle \mathcal{E}^{*N}(t_1)\mathcal{E}^{N}(t_2)\right\rangle \langle\rho_{ii}(t_2)\rangle$. However, there are specific models of fluctuating fields where the decorrelation is mathematically rigorous and does not stand only as an approximation. In the following, we will describe two well-known and mostly used models for stochastic fields, namely the phase-diffusion and the chaotic field model.

In the phase-diffusion (PD) model the field has non-fluctuating amplitude but its phase is a Wiener-Levy stochastic process [18]. In this case the nth-order correlation

function of the field is equal to [19]:

$$\langle \varepsilon^*(t_1)\varepsilon(t_2)...\varepsilon^*(t_{2n-1})\varepsilon(t_{2n})\rangle = \prod_{j\to odd}^{2n-1} \langle \varepsilon^*(t_j)\varepsilon(t_{j+1})\rangle \tag{3.1}$$

with $t_j > t_{j+1}$.

This represents a Markovian process, with an exponential first-order correlation function given by [18]:

$$\langle \varepsilon^*(t_1)\varepsilon(t_2)\rangle = \left\langle |\varepsilon(t)|^2 \right\rangle \exp[-\frac{1}{2}\gamma_L \left|t_1 - t_2\right|] \tag{3.2}$$

where γ_L is the bandwidth of the field. The mean value of the field amplitude in the PD model is zero, i.e. $\langle \mathcal{E}(t)\rangle = 0$.

It has been established [17] that, in the case of the phase-diffusion model, the decorrelation of the atom-field dynamics is rigorous without any approximation. Physically, this is easy to understand, because for a constant amplitude, the fluctuations of the phase of the field cannot affect the evolution of the populations, but only the coherence, which means the relative phase of the coefficients representing the superposition of the states coupled by the field. And it is the correlation between the time evolution of populations that is factorized in the process of decorrelation. Formally, the decorrelation is justified due to the statistical independence of the increments of a Wiener-Levy process. If $f(\ \varphi_1 \ \ ... \ \ \varphi_n\ ;\ t_1 \ \ ... \ \ t_n\ )$, $t_1 > t_2 > ... > t_n = 0$ is the joint probability density of the infinite set of random variables $\varphi_j = \varphi(t_j)$ and $f(\varphi_1, t_1|\varphi_2, t_2) = \frac{f(\ \varphi_1 \ \ ... \ \ \varphi_n\ ;\ t_1 \ \ ... \ \ t_n\ )}{f(\ \varphi_2 \ \ ... \ \ \varphi_n\ ;\ t_2 \ \ ... \ \ t_n\ )} = \frac{1}{[2\pi\gamma(t_1-t_2)]^{1/2}} e^{-\frac{(\varphi_1-\varphi_2)^2}{2\gamma(t_1-t_2)}}$ the conditional probability density of the Markov process $\varphi(t)$, then we can write:

$$\begin{aligned}
\langle \omega_R^*(t_1)\omega_R(t_2)n(t_2)\rangle = & \int_{-\infty}^{\infty} d\varphi_1 \ \ ... \ \ \int_{-\infty}^{\infty} d\varphi_n \ f(\ \varphi_1 \ \ ... \ \ \varphi_n\ ;\ t_1 \ \ ... \ \ t_n\ )\bar{\omega}_R^2 \\
& \times e^{-i(\varphi_1-\varphi_2)} n(\ \varphi_2 \ \ ... \ \ \varphi_n\ ) \\
& = (\bar{\omega}_R^2(t_2) \int_{-\infty}^{\infty} d\varphi_1 f(\varphi_1, t_1|\varphi_2, t_2) e^{-i(\varphi_1-\varphi_2)}) \\
\times (& \int_{-\infty}^{\infty} d\varphi_2 \ \ ... \ \ \int_{-\infty}^{\infty} d\varphi_n \ f(\ \varphi_2 \ \ ... \ \ \varphi_n\ ;\ t_2 \ \ ... \ \ t_n\ ) n(\ \varphi_2 \ \ ... \ \ \varphi_n\ )) \\
& = \langle \omega_R^*(t_1)\omega_R(t_2)\rangle \langle n(t_2)\rangle
\end{aligned} \tag{3.3}$$

In the chaotic field model the field undergoes both amplitude and phase fluctuations. Its amplitude is a complex Gaussian stochastic process with its nth order correlation function obeying [19]:

$$\langle \varepsilon^*(t_1)\varepsilon(t_2)...\varepsilon^*(t_{2n-1})\varepsilon(t_{2n})\rangle = \sum_P \prod_{j\to odd}^{2n-1} \left\langle \varepsilon^*(t_j)\varepsilon(t_{P(j+1)})\right\rangle \tag{3.4}$$

where the sum is over all possible permutations P, with $t_j > t_{j+1}$. The field amplitude is usually written in the form $\mathcal{E}(t) = \mathcal{E}_x(t) + i\mathcal{E}_y(t)$, where $\mathcal{E}_x(t)$ and $\mathcal{E}_y(t)$ are two independent Gaussian processes with mean values equal to zero. For the sake of

simplicity we will assume the chaotic field to be Markovian , something that it is not necessarily satisfied for a general chaotic field. In this case the first-order correlation function of the field is given by equation (3.2).

Contrary to the case of the phase diffusion model, the decorrelation of atomic-field dynamics is not mathematically rigorous for a chaotic field, but stands only as an approximation, valid in the weak field regime. The relative errors of this approximation have been evaluated in a very interesting recent theoretical work [20] that also includes systematical methods of describing fluctuating SASE-FEL pulses and their coupling to a singe Auger resonance .

3.2 Time evolution of a two-level system subject to an external stochastic field

In this section we solve the problem of the time evolution of a two-level system driven by a stochastic electric field [2]. We begin by considering a two-level atom with a ground state $|1\rangle$ and an excited state $|2\rangle$ subject to an electric field of the form $E(t) = \mathcal{E}(t)e^{i\omega t} + \mathcal{E}^*(t)e^{-i\omega t}$. The complex field amplitude is generally assumed to undergo fluctuations and can be written in the form $\mathcal{E}(t) \equiv |\mathcal{E}(t)|\, e^{i\varphi(t)}$, with $|\mathcal{E}(t)|$ and $\varphi(t)$ the real amplitude and the phase of the field, respectively. The electric dipole between the two states is μ_{12} and the transition frequency ω_{21}. The equations of motion of the density matrix in the RWA are

$$(\frac{d}{dt} + i\Delta + \frac{1}{2}\Gamma_{21})\sigma_{12}(t) = \frac{1}{2}i\omega_R(t)n(t) \tag{3.5}$$

$$(\frac{d}{dt} + \Gamma_2)n(t) = -\Gamma_2 - 2\mathrm{Im}[\omega_R^*(t)\sigma_{12}(t)] \tag{3.6}$$

where we introduced the slowly varying amplitudes $\rho_{ii}(t) = \sigma_{ii}(t)$, $i = 1, 2$ and $\rho_{12}(t) = \sigma_{12}(t)e^{i\omega t}$. By $n(t) = \sigma_{22}(t) - \sigma_{11}(t)$, we denote the population difference and by Δ the detuning from the resonance, i.e. $\Delta = \omega - \omega_{21}$. Γ_2 is the spontaneous decay rate of the excited state, while Γ_{21} the off-diagonal relaxation that may include decays other than Γ_2 as for example in the case of elastic collisions. The Rabi frequency $\omega_R(t) = 2\hbar^{-1}\mu_{12}\mathcal{E}(t)$ is stochastic and its mean value will be denoted by $\bar{\omega}_R(t) = 2\hbar^{-1}\mu_{12}\mathcal{E}_0$. Since the system is closed, the populations satisfy the normalization condition $\sigma_{11}(t) + \sigma_{22}(t) = 1$.

We integrate both equations formally and eliminate $\sigma_{12}(t)$ to obtain:

$$n(t) = -1 - \mathrm{Re}\int_0^t e^{\Gamma_2(t_1-t)}dt_1 \times \int_0^{t_1} e^{(i\Delta+\frac{1}{2}\Gamma_{21})(t_2-t_1)}\omega_R^*(t_1)\omega_R(t_2)n(t_2)dt_2 \tag{3.7}$$

where the initial conditions $\sigma_{11}(0) = 1$, $\sigma_{22}(0) = 1$ and $\sigma_{12}(0) = 0$ were used.

3.2.1 Phase-Diffusion Field

We will now assume that the model of the field is the phase-diffusion described above, therefore the stochastic average of eqn. (3.6) over the fluctuating phase, in view of eqn. (3.2) will yield:

$$\langle n(t)\rangle = -1 - \mathrm{Re}\int_0^t e^{\Gamma_2(t_1-t)}dt_1 \times \int_0^{t_1} e^{(i\Delta+\frac{1}{2}\Gamma_{21}+\gamma)(t_2-t_1)}\bar{\omega}_R^2(t_2)\,\langle n(t_2)\rangle\, dt_2 \tag{3.8}$$

where γ the field bandwidth. We now take the Laplace transform of both sides of eqn.(3.8) and find:

$$\langle N(p)\rangle = -\frac{1}{p} - \mathrm{Re}\left\{ \frac{\bar{\omega}_R^2}{(p+\Gamma_2)\left[p + i\Delta + \frac{1}{2}(\Gamma_{21}+\gamma)\right]} \langle N(p)\rangle \right\} \tag{3.9}$$

where with $\langle N(p)\rangle$ we denoted the Laplace transform of $\langle n(t)\rangle$. The steady state value of the population difference can be evaluated using the final value theorem for the Laplace transform, namely $\lim_{p\to 0} p\langle N(p)\rangle = \langle n(t=\infty)\rangle$. Using this theorem one obtains:

$$\langle n\rangle^{PD} = -1/(1+S) \tag{3.10}$$

where S is the saturation parameter given by

$$S = \frac{(\bar{\omega}_R^2/\Gamma_2)\frac{1}{2}(\Gamma_{21}+\gamma)}{\Delta^2 + \frac{1}{4}(\Gamma_{21}+\gamma)^2} \tag{3.11}$$

Therefore we can see that the only change that the fluctuating phase is introducing, is the addition of the field bandwidth to the atomic linewidth Γ_{21}. The expression for the averaged population of the second state is

$$\langle \sigma_{22}\rangle^{PD} = \frac{\frac{1}{2}S}{1+S} = \frac{\frac{1}{4}(\Gamma_{21}+\gamma)^2}{\frac{\Delta^2}{1+S_0} + \frac{1}{4}(\Gamma_{21}+\gamma)^2} \frac{\frac{1}{2}S_0}{1+S_0} \tag{3.12}$$

where S_0 is the value of S when the field is exactly on resonance with the $|1\rangle \leftrightarrow |2\rangle$ transition. The profile of eqn. (3.12) is Lorentzian with FWHM equal to $\sqrt{1+S_0}(\Gamma_{21}+\gamma)$.

3.2.2 Chaotic Field

If the field is chaotic, then the stochastic average of eqn. (3.7) is generally a challenging task. Therefore one has to obtain a perturbation series expansion for the correction to the decorrelation approximation [2]. Only in the case of zero bandwidth the exact correction can be found. Note that $\gamma = 0$ implies an infinite correlation time and the field is random with statistics independent of time. In this case the phase of the field has a uniform distribution from 0 to 2π and its real amplitude has a Rayleigh distribution. Hence, the stochastic average is given by:

$$\langle n(t)\rangle = \int_0^{2\pi}\int_0^{\infty} \frac{2\,|\omega_R|\, e^{-\left(\frac{|\omega_R|}{\bar{\omega}_R}\right)^2}}{2\pi\bar{\omega}_R^2} n\left(|\omega_R|, \varphi, t\right) d\,|\omega_R|\, d\varphi \tag{3.13}$$

Taking the derivative of both sides of eqn. (3.13) with respect to $\bar{\omega}_R^2 = \langle \omega_R^* \omega_R\rangle$ one finds:

$$\langle \omega_R^* \omega_R n(t)\rangle = \langle \omega_R^*\omega_R\rangle \langle n(t)\rangle + \langle \omega_R^*\omega_R\rangle^2 \frac{d\langle n(t)\rangle}{d\langle \omega_R^*\omega_R\rangle} \tag{3.14}$$

If we move the first term of the right-hand side of equation (3.14) to left-side, we can see that the second term is equal to $\langle \omega_R^*\omega_R \delta n(t)\rangle$ which represents the correlation between the intensity of the chaotic field and the fluctuations of the population difference around its mean value, i.e. $\delta n(t) = n(t) - \langle n(t)\rangle$. Using eqn. (3.14) the

stochastic average of eqn. (3.7) leads to the relation

$$S^2 \frac{d\langle n\rangle}{dS} + (1+S)\langle n\rangle + 1 = 0 \tag{3.15}$$

where S is given by eqn. (3.11) with $\gamma = 0$. Equation (3.15) is differential and its solution can be written in the various forms:

$$\langle n\rangle^{CH} = -\frac{e^{1/S}}{S}\int_1^\infty \frac{e^{-t/S}}{t}dt \equiv -\frac{e^{1/S}}{S}E_1(1/S) = \int_0^\infty \left(\frac{-1}{1+S'}\right)\frac{e^{-S'/S}}{S}dS' \tag{3.16}$$

Equation (3.16) indicates that the mean value of the population difference of a chaotic field with zero bandwidth can be calculated by first finding the solution for a coherent field, i.e. phase-diffusion field with zero bandwidth, and then average the result over the exponential intensity distribution of the chaotic field.

For $S \ll 1$ the asymptotic expansion of $E_1(1/S)$ results $\langle n\rangle^{CH} = -\sum_{k=0}^{\infty} k!(-S)^k$ while in the case of the phase-diffusion field $\langle n\rangle^{PD} = -\sum_{k=0}^{\infty}(-S)^k$. The two results agree only to first order perturbation theory. For $S \gg 1$ the series expansion of $E_1(1/S)$ leads to the result $\langle n\rangle^{CH} \simeq -(\ln S)/S$ while $\langle n\rangle^{PD} \simeq -1/S$. This indicates that the chaotic field is less effective in saturating a one-photon transition than a coherent field.

We now consider the more complex case of arbitrary bandwidth, where a non-perturbative relation between $\langle \omega_R^*(t_1)\omega_R(t_2)n(t_2)\rangle$ and $\langle n(t_2)\rangle$ cannot be found by simply knowing the statistics of the Rabi frequency. For Markovian chaotic fields one can show that $\langle \omega_R^*(t_1)\omega_R(t_2)n(t_2)\rangle = \exp\left[-\frac{1}{2}\gamma(t_1-t_2)\right]\langle \omega_R^*(t_2)\omega_R(t_2)n(t_2)\rangle$ but no further progress can be made. However, using a systematic method presented here, we can develop a perturbation series of the correlation $\langle \omega_R^*(t_1)\omega_R(t_2)n(t_2)\rangle$ that can be summed to all orders [2]. We begin by writing $n(t) = \langle n(t)\rangle + \delta n(t)$, which also implies $\langle \delta n(t)\rangle = 0$. Substituting this relation back to (3.7) and taking the stochastic average one finds:

$$\langle n(t)\rangle = -1 - \mathrm{Re}\int_0^t e^{\Gamma_2(t_1-t)}dt_1 \int_0^{t_1} e^{\left[(i\Delta+\frac{1}{2}\Gamma_{21})(t_2-t_1)\right]}$$

$$\times\left[\langle \omega_R^*(t_1)\omega_R(t_2)\rangle\langle n(t_2)\rangle + \langle \omega_R^*(t_1)\omega_R(t_2)\delta n(t_2)\rangle\right]dt_2 \tag{3.17}$$

Subtracting eqn. (3.17) from eqn. (3.7), one gets:

$$\delta n(t_2) = -\mathrm{Re}\int_0^{t_2} e^{\Gamma_2(t_3-t_2)}dt_3 \int_0^{t_3} e^{\left[(i\Delta+\frac{1}{2}\Gamma_{21})(t_4-t_3)\right]}$$

$$\times\left\{\left[\omega_R^*(t_3)\omega_R(t_4) - \langle \omega_R^*(t_3)\omega_R(t_4)\rangle\right]\langle n(t_4)\rangle\right.$$

$$\left.+\left[\omega_R^*(t_3)\omega_R(t_4)\delta n(t_4) - \langle \omega_R^*(t_3)\omega_R(t_4)\delta n(t_4)\rangle\right]dt_4\right. \tag{3.18}$$

Iterating eqn. (3.18) and eliminating $\delta n(t_2)$ in eqn. (3.17) we find the following series integral equation:

$$\langle n(t)\rangle = -1 - \mathrm{Re}\int_0^t e^{\Gamma_2(t_1-t)}dt_1 \int_0^{t_1} e^{\left[(i\Delta+\frac{1}{2}\Gamma_{21})(t_2-t_1)\right]}dt_2$$

$$\times[\langle\omega_R^*(t_1)\omega_R(t_2)\rangle\,\langle n(t_2)\rangle - \mathrm{Re}\int_0^{t_2} e^{\Gamma_2(t_3-t_2)}dt_3\int_0^{t_3} e^{\left[(i\Delta+\frac{1}{2}\Gamma_{21})(t_4-t_3)\right]}dt_4$$

$$\times(\langle\omega_R^*(t_1)\omega_R(t_4)\rangle\,\langle\omega_R^*(t_3)\omega_R(t_2)\rangle\,\langle n(t_4)\rangle - \mathrm{Re}\int_0^{t_4} e^{\Gamma_2(t_5-t_4)}dt_5\int_0^{t_5} e^{\left[(i\Delta+\frac{1}{2}\Gamma_{21})(t_6-t_5)\right]}dt_6$$

$$\times[\langle\omega_R^*(t_1)\omega_R(t_6)\rangle\,\langle\omega_R^*(t_3)\omega_R(t_4)\rangle\,\langle\omega_R^*(t_5)\omega_R(t_2)\rangle$$

$$+\langle\omega_R^*(t_1)\omega_R(t_4)\rangle\,\langle\omega_R^*(t_3)\omega_R(t_6)\rangle\,\langle\omega_R^*(t_5)\omega_R(t_2)\rangle$$

$$+\langle\omega_R^*(t_1)\omega_R(t_6)\rangle\,\langle\omega_R^*(t_3)\omega_R(t_2)\rangle\,\langle\omega_R^*(t_5)\omega_R(t_4)\rangle\,\langle n(t_6)\rangle - ...])] \tag{3.19}$$

Since we assumed that the field is Markovian, its first order correlation function is exponential and the above equation is generally solvable using the Laplace transform. However due to the complexity of equation (3.19) one should develop a systematic way of calculating its Laplace transform. One useful way it to express our equation in terms of diagrams [21, 22]:

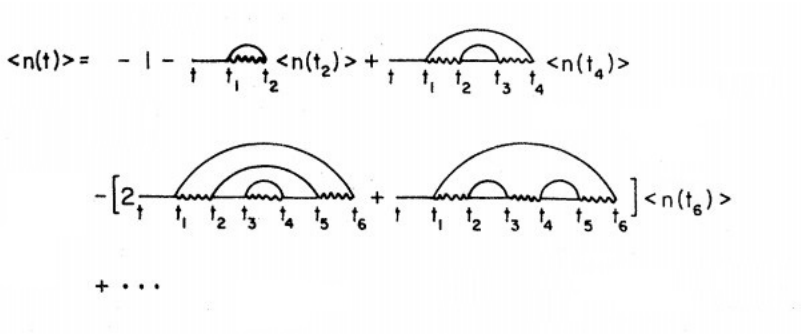

FIGURE 3.1: Diagram Representation of equation (3.19) [2]

where the straight line between two successive vertices at t_j and t_{j+1} is associated with the factor $\exp\left[\Gamma_2(t_{j+1}-t_j)\right]$ while the wavy line with the factor $\frac{1}{2}\exp\left[\left(i\Delta+\frac{1}{2}\Gamma_{21}\right)(t_{j+1}-t_j)\right]+c.c.$ A loop connecting two vertices at t_j and t'_j, with $t_j > t'_j$ and $j < j'$ is associated with the factor $\bar{\omega}_R^2\exp\left[-\frac{1}{2}\gamma(t_j-t'_j)\right]$. We will call t_j and t'_j the initial and the final vortex of the loop, respectively. It is important to notice that although eqn. (3.19) may contain intersecting loops, the exponential form of the first-order correlation function allows us to replace these loops by non-intersecting ones. In example, the part of the diagram that represents the term $\langle\omega_R^*(t_1)\omega_R(t_4)\rangle\,\langle\omega_R^*(t_3)\omega_R(t_6)\rangle\,\langle\omega_R^*(t_5)\omega_R(t_2)\rangle$ can be replaced equivalently by $\langle\omega_R^*(t_1)\omega_R(t_6)\rangle\,\langle\omega_R^*(t_3)\omega_R(t_4)\rangle\,\langle\omega_R^*(t_5)\omega_R(t_2)\rangle$. Taking the Laplace transform of the diagram of figure 3.1 and applying the frequency-shift theorem we find:

$$\langle N(p)\rangle = -(1/p)/\left[1+\sum\nolimits_1(p)\right] \tag{3.20}$$

where

$$\sum\nolimits_1(p) = \mathrm{Re}\frac{\bar{\omega}_R^2}{(p+\Gamma_2)\left[p+i\Delta+\frac{1}{2}(\Gamma_{21}+\gamma)\right]}\times\left(1-\mathrm{Re}\frac{\bar{\omega}_R^2}{(p+\Gamma+\gamma)\left[p+i\Delta+\frac{1}{2}(\Gamma_{21}+\gamma)\right]}+...\right)$$

$$\equiv \mathrm{Re}\frac{\bar{\omega}_R^2}{(p+\Gamma_2)\left[p+i\Delta+\frac{1}{2}(\Gamma_{21}+\gamma)\right]}\frac{1}{1+\sum_2(p)} \tag{3.21}$$

Equation (3.21) also defines $\sum_2(p)$. The recursion relation between the functions $\sum_i(p)$ is

$$\sum\nolimits_m(p) = \frac{S_m(p)}{1+\sum_{m+1}(p)} \tag{3.22}$$

with

$$S_m(p) = Re\frac{(m+1)\bar{\omega}_R^2}{2\left[p+\Gamma_2+\frac{1}{2}(m-1)\gamma\right]\left[p+i\Delta+\frac{1}{2}(\Gamma_{21}+m\gamma)\right]} \tag{3.23}$$

for m odd, or

$$S_m(p) = Re\frac{m\bar{\omega}_R^2}{2\left(p+\Gamma_2+\frac{1}{2}m\gamma\right)\left\{p+i\Delta+\frac{1}{2}\left[\Gamma_{21}+(m-1)\gamma\right]\right\}} \tag{3.24}$$

for m even. The coefficients S_m are called saturation coefficients. The steady state value of the population difference is given by

$$\langle n\rangle^{CH} = -\frac{1}{1+\sum_1} = \frac{-1}{1+\frac{S_1}{1+\frac{S_2}{1+\ldots}}} \tag{3.25}$$

where $\sum_m$ and S_m are given by equations (3.22), (3.23) and (3.24) by applying $p=0$. The first saturation coefficient S_1 is identical to the saturation parameter defined in eqn. (3.11) for the case of the phase-diffusion field. Therefore the relation $\sum_1 < S_1$ implies the known result, that a chaotic field is always less effective in saturating a one-photon transition than a phase-diffusion field. If we set $\gamma = 0$ in eqn. (3.25) we get the continued fraction result $-\frac{e^{1/S}}{S}E_1(1/S)$ of eqn. (3.16). For non-zero bandwidth eqn. (3.25) converges and can be suitably truncated and summed to any desired accuracy.

Chapter 4

Autoionizing States driven by Stochastic fields

In this section we will provide a theoretical description of the problem of an AIS subject to an external fluctuating electromagnetic field as well as the basic results of this study. The theory will be cast in terms of the density matrix operator, since this formalism is suitable for taking into account the stochastic properties of the radiation field.

4.1 Theory

We begin by considering a two-level atom whose ground state $|1\rangle$ is coupled to an isolated autoionizing state (AIS) $|2\rangle$ via a single-photon transition, in the presence of an external electric field $E(t) = \frac{1}{2}[\mathcal{E}(t)e^{i\omega t} + c.c.]$. Its frequency ω is tuned around the resonant frequency $\omega_{21} \equiv \omega_2 - \omega_1$ and $\mathcal{E}(t) = |\mathcal{E}(t)| \exp[i\varphi(t)]$ is in general assumed to undergo stochastic fluctuations. The coupling to the resonance is characterized by the complex Rabi frequency $\tilde{\Omega}(t) = \Omega(t)(1 - \frac{i}{q}) = \frac{1}{2}\mathcal{E}(t)d_{21}(1 - \frac{i}{q})$, where d_{21} is the electric dipole matrix element between the ground state and the discreet part of the resonance and q the asymmetry parameter [13]. The ground state is also coupled directly to the continuum via a dipole matrix element accounting for ionization into the smooth continuum, leading to an ionization width denoted by $\gamma(t)$. The autoionization width Γ represents the rate of decay of the AI state due to the Coulomb interaction between the two excited electrons. Spectroscopically it appears as the width of the excitation profile of the resonance and it is equal to the inverse of the lifetime of the AIS. The q parameter accounts for the interference between the two paths to the continuum; the direct and the one via the discreet part.

Depending on the aspects of the problem to be addressed, the theory can be cast either in terms of the time-dependent Schröndinger equation or the density matrix. Since one of our objectives is to account for the effect of field fluctuations, we need the density matrix $\rho(t)$, within the rotating wave approximation (RWA). The dynamical evolution of its slowly varying part $\sigma(t)$ is expressed by the following equations (see Chapter 2.2.3):

$$\partial_t \sigma_{11}(t) = -\gamma(t)\sigma_{11}(t) + 2Im\left\{\Omega(t)\left(1 - \frac{i}{q}\right)\sigma_{21}(t)\right\} \tag{4.1}$$

$$\partial_t \sigma_{22}(t) = -\Gamma\sigma_{22}(t) - 2Im\left\{\Omega(t)\left(1 + \frac{i}{q}\right)\sigma_{21}(t)\right\} \tag{4.2}$$

$$\left[\partial_t - i\Delta + \frac{1}{2}\left(\gamma(t) + \Gamma\right)\right]\sigma_{21}(t) = -i\Omega(t)\left(1 - \frac{i}{q}\right)\sigma_{11}(t) + i\Omega(t)\left(1 + \frac{i}{q}\right)\sigma_{22}(t) \tag{4.3}$$

where we have introduced the slowly varying amplitudes $\sigma_{ij}(t)$, obeying $\rho_{ii}(t) = \sigma_{ii}(t)$, $i = 1, 2$ and $\rho_{21}(t) = \sigma_{21}(t)exp[i\omega t]$. The detuning Δ of the photon frequency from resonance is defined by $\Delta \equiv \omega - \omega_{21}$. Note that the left side of equation (4.3) may in general contain additional coherence (off-diagonal) relaxation constants which are of no relevance to our problem, in the case of monochromatic field. However, a coherence relaxation constant appears below, as we introduce field fluctuations.

The matrix elements of the density matrix in the above equations are generally fluctuating variables owing to the stochastic character of the field which imparts fluctuations to the Rabi frequency and the ionization width. We are therefore dealing with stochastic differential equations. The observed quantities which refer to the atom are given by the average over the stochastic fluctuations of the field. This requires a realistic model of the stochastic properties of the field, or a brute force numerical integration over trajectories imitating the the fluctuations of the field. For the time being, we will work within the first approach.

To this end, we solve equation (4.3) for $\sigma_{21}(t)$ formally, and substitute into equations (4.1) and (4.2). Then taking the stochastic averages of the resulting equations and obtain:

$$\partial_t \langle\sigma_{11}(t)\rangle = -\langle\gamma(t)\sigma_{11}(t)\rangle + 2\mathrm{Im}\left\{\left(1-\frac{i}{q}\right)\int_0^t -i\left(1-\frac{i}{q}\right)\langle\Omega(t)\Omega(t')\sigma_{11}(t')\rangle\, e^{-\kappa(t-t')}dt'\right.$$
$$\left. + \left(1-\frac{i}{q}\right)\int_0^t i\left(1+\frac{i}{q}\right)\langle\Omega(t)\Omega(t')\sigma_{22}(t')\rangle\, e^{-\kappa(t-t')}dt'\right\} \tag{4.4}$$

$$\partial_t \langle\sigma_{22}(t)\rangle = -\Gamma\langle\sigma_{22}(t)\rangle - 2\mathrm{Im}\left\{\left(1+\frac{i}{q}\right)\int_0^t -i\left(1-\frac{i}{q}\right)\langle\Omega(t)\Omega(t')\sigma_{11}(t')\rangle\, e^{-\kappa(t-t')}dt'\right.$$
$$\left. + \left(1+\frac{i}{q}\right)\int_0^t i\left(1+\frac{i}{q}\right)\langle\Omega(t)\Omega(t')\sigma_{22}(t')\rangle\, e^{-\kappa(t-t')}dt'\right\} \tag{4.5}$$

where we defined $\kappa \equiv -i\Delta + \frac{1}{2}(\gamma + \Gamma)$.

Equations (4.4) and (4.5) involve atom-field correlation functions of the form $\langle\Omega(t)\Omega(t')\sigma_{ii}(t')\rangle$, $i = 1, 2$. Generally such correlation functions cannot be evaluated without knowing the specific form of the fluctuations of the field. As an approximation valid under certain conditions, one could decorrelate the atomic-field dynamics by taking $\langle\Omega(t)\Omega(t')\sigma_{ii}(t')\rangle = \langle\Omega(t)\Omega(t')\rangle\langle\sigma_{ii}(t')\rangle$. However, as discussed in detail, there are specific models of fluctuating fields where the decorrelation is mathematically rigorous and does not stand only as an approximation.

In view of the discussion in section 3, we proceed with the decorrelation of the atomic-field dynamics, with the resulting equations being exact for the PD model and valid in the weak-moderate field limit for the chaotic model. Note that the decorrelation of the product $\langle\gamma(t)\sigma_{11}(t)\rangle$ is rigorous for the PD model, since $\gamma(t)$ is proportional to the intensity which does not undergo fluctuations. In the chaotic field model this decorrelation is valid within the DA since the intensity is replaced by its averaged value. After the decorrelation, equations (4.4) and (4.5) become:

$$\partial_t \langle\sigma_{11}(t)\rangle = -\langle\gamma(t)\rangle \langle\sigma_{11}(t)\rangle + d_{12}^2 I(t) \mathrm{Im}\left\{ \left(1-\frac{i}{q}\right) \int_0^t -i \left(1-\frac{i}{q}\right) \langle\sigma_{11}(t')\rangle e^{-\tilde{\kappa}(t-t')} dt' \right.$$

$$\left. + \left(1-\frac{i}{q}\right) \int_0^t i \left(1+\frac{i}{q}\right) \langle\sigma_{22}(t')\rangle e^{-\tilde{\kappa}(t-t')} dt' \right\} \tag{4.6}$$

$$\partial_t \langle\sigma_{22}(t)\rangle = -\Gamma \langle\sigma_{22}(t)\rangle - d_{12}^2 I(t) \mathrm{Im}\left\{ \left(1+\frac{i}{q}\right) \int_0^t -i \left(1-\frac{i}{q}\right) \langle\sigma_{11}(t')\rangle e^{-\tilde{\kappa}(t-t')} dt' \right.$$

$$\left. + \left(1+\frac{i}{q}\right) \int_0^t i \left(1+\frac{i}{q}\right) \langle\sigma_{22}(t')\rangle e^{-\tilde{\kappa}(t-t')} dt' \right\} \tag{4.7}$$

where we have substituted the complete expression of the Rabi frequency $\Omega(t) = \frac{1}{2}\mathcal{E}(t)d_{21}$ and defined $\tilde{\kappa} \equiv \kappa + \frac{1}{2}\gamma_L = -i\Delta + \frac{1}{2}(\gamma + \Gamma + \gamma_L)$. In the RWA, the intensity appearing in equations (4.6) and (4.7) is expressed in terms of the field amplitude as $I(t) = \frac{\langle|\mathcal{E}(t)|^2\rangle}{2}$.

Let us consider, for the moment, the case of constant intensity $I(t) = I_0$, which leads to considerable simplification enabling analytical solutions. Since the integrals appearing in (4.6) and (4.7) are with respect to the time t, which is a real variable, the interchange of the Imaginary (or Real) part and integration are mathematically rigorous. Using this fact and expanding the exponential functions in the integrands in terms of Cosine and Sine functions, we obtain:

$$\partial_t \langle\sigma_{11}(t)\rangle = -\gamma \langle\sigma_{11}(t)\rangle + d_{12}^2 I_0 \left(-1+\frac{1}{q^2}\right) \int_0^t \langle\sigma_{11}(t')\rangle e^{-\frac{1}{2}(\gamma+\Gamma+\gamma_L)(t-t')} \cos[\Delta(t-t')] dt'$$

$$+ d_{12}^2 I_0 \left(-\frac{2}{q}\right) \int_0^t \langle\sigma_{11}(t')\rangle e^{-\frac{1}{2}(\gamma+\Gamma+\gamma_L)(t-t')} \sin[\Delta(t-t')] dt'$$

$$+ d_{12}^2 I_0 \left(1+\frac{1}{q^2}\right) \int_0^t \langle\sigma_{22}(t')\rangle e^{-\frac{1}{2}(\gamma+\Gamma+\gamma_L)(t-t')} \cos[\Delta(t-t')] dt' \tag{4.8}$$

$$\partial_t \langle\sigma_{22}(t)\rangle = -\Gamma \langle\sigma_{22}(t)\rangle - d_{12}^2 I_0 \left(-1-\frac{1}{q^2}\right) \int_0^t \langle\sigma_{11}(t')\rangle e^{-\frac{1}{2}(\gamma+\Gamma+\gamma_L)(t-t')} \cos[\Delta(t-t')] dt'$$

$$- d_{12}^2 I_0 \left(-\frac{2}{q}\right) \int_0^t \langle\sigma_{22}(t')\rangle e^{-\frac{1}{2}(\gamma+\Gamma+\gamma_L)(t-t')} \sin[\Delta(t-t')] dt'$$

$$- d_{12}^2 I_0 \left(1-\frac{1}{q^2}\right) \int_0^t \langle\sigma_{22}(t')\rangle e^{-\frac{1}{2}(\gamma+\Gamma+\gamma_L)(t-t')} \cos[\Delta(t-t')] dt' \tag{4.9}$$

Note that for constant intensity, the width of the direct ionization to the continuum is also constant, i.e $\gamma(t) = \gamma$. The integrals appearing in equations (4.8) and (4.9) are now convolutions of $\langle\sigma_{ii}(t')\rangle$, $i = 1, 2$ and the Sin/Cosine functions.
Taking now the Laplace transforms of the above equations we obtain:

$$sF_1(s) = -\gamma F_1(s) + d_{12}^2 I_0 \left[\left(-1 + \frac{1}{q^2} \right) F_1(s)G_1(s) - \frac{2}{q} F_1(s)G_2(s) + \left(1 + \frac{1}{q^2} \right) F_2(s)G_1(s) \right] \tag{4.10}$$

$$sF_2(s) = -\Gamma F_2(s) - d_{12}^2 I_0 \left[\left(-1 - \frac{1}{q^2} \right) F_1(s)G_1(s) - \frac{2}{q} F_2(s)G_2(s) + \left(1 - \frac{1}{q^2} \right) F_2(s)G_1(s) \right] \tag{4.11}$$

where $F_1(s)$ and $F_2(s)$ are the Laplace transforms of $\langle \sigma_{11}(t) \rangle$ and $\langle \sigma_{22}(t) \rangle$, while $G_1(s)$ and $G_2(s)$ are the Laplace transforms of the functions $g_1(t) = e^{-\frac{1}{2}(\gamma+\Gamma+\gamma_L)t} \cos(\Delta t)$ and $g_2(t) = e^{-\frac{1}{2}(\gamma+\Gamma+\gamma_L)t} sin(\Delta t)$, respectively. It is straightforward to show that

$$G_1(s) = \frac{s + \frac{1}{2}(\gamma + \Gamma + \gamma_L)}{\left[s + \frac{1}{2}(\gamma + \Gamma + \gamma_L) \right]^2 + \Delta^2} \tag{4.12}$$

$$G_2(s) = \frac{\Delta}{\left[s + \frac{1}{2}(\gamma + \Gamma + \gamma_L) \right]^2 + \Delta^2} \tag{4.13}$$

The system of equations (12) and (13) can easily be solved for $F_1(s)$ and $F_2(s)$, the inverse Laplace transform of which give us the exact time dependence of $\langle \sigma_{11}(t) \rangle$ and $\langle \sigma_{22}(t) \rangle$. The expressions are too lengthy and complicated to be enlightening, but the results are discussed in later sections.

Returning now to the more general case of time-dependent intensity $I(t)$, the above analytical treatment using the Laplace transform does not lead to helpful expressions and even the numerical solution of equations (4.6) and (4.7) tends to be a very difficult task. However, useful insight can be gained through the approximation,

$$\langle \sigma_{ii}(t') \rangle \simeq \langle \sigma_{ii}(t' = t) \rangle \qquad i = 1, 2 \tag{4.14}$$

which is valid in the weak field limit. Its validity rests on the realization that, under weak driving, the populations do not change significantly, over times of rapid oscillations of the rest of the integrand. As a result they can be evaluated at times $t' = t$ and factored out of the integral. In that case, the integration with respect to t' in equations (4.6) and (4.7) can be performed, leading to the somewhat simplified system of differential (rate) equations,

$$\partial_t \langle \sigma_{11}(t) \rangle = -\gamma(t) \langle \sigma_{11}(t) \rangle + d_{12}^2 I(t) \mathrm{Im} \left\{ (-i) \left(1 - \frac{i}{q} \right)^2 \frac{1 - e^{-\tilde{\kappa} t}}{\tilde{\kappa}} \langle \sigma_{11}(t) \rangle + i \left(1 - \frac{i}{q} \right) \left(1 + \frac{i}{q} \right) \frac{1 - e^{-\tilde{\kappa} t}}{\tilde{\kappa}} \langle \sigma_{22}(t) \rangle \right\} \tag{4.15}$$

$$\partial_t \langle \sigma_{22}(t) \rangle = -\Gamma \langle \sigma_{22}(t) \rangle - d_{12}^2 I(t) \mathrm{Im} \left\{ (-i) \left(1 - \frac{i}{q} \right) \left(1 + \frac{i}{q} \right) \frac{1 - e^{-\tilde{\kappa} t}}{\tilde{\kappa}} \langle \sigma_{11}(t) \rangle \right.$$

$$+i\left(1+\frac{i}{q}\right)^2\frac{1-e^{-\tilde{\kappa}t}}{\tilde{\kappa}}\langle\sigma_{22}(t)\rangle\Bigg\} \tag{4.16}$$

The system of equations (4.15) and (4.16) can now be solved numerically in the limit of weak field, as long as the the system is well below saturation. Actually, for special forms of the time dependent $I(t)$, analytical solutions may also exist.

We note that the method described in section 3.1.2 is not directly applicable to our problem. The basic reasons are two: The first is that our system is not closed, therefore the relation $\sigma_{11}(t)+\sigma_{22}(t)=1$ which simplifies the problem a lot, is not satisfied. The second and primary reason is that, due to the complex character of the Rabi frequency, it is impossible to reduce the problem to a differential equation describing the time evolution of the population difference. Therefore application of the method described in 3.1.2 would lead to two equations similar to (3.18), describing the time evolution of fluctuations of the population of each state ($\delta\sigma_{11}(t)$, $\delta\sigma_{22}(t)$) which are also coupled. The elimination of these fluctuations (see eqn. (3.19)) leads to extremely complicated expressions which are marginally impossible to be handled even with the diagram method described in chapter 3.

4.2 Results and Discussion

In this section we present the main results of our theoretical research on AIS in stochastically fluctuating fields. We apply our theory to the case of Helium 2s2p $^1P^0$ AIS which offers a perfect example of an isolated auto-ionizing resonance.

We begin by solving the system of equations (4.10) and (4.11) and inverting the Laplace transforms to find the expressions for $\langle\sigma_{11}(t)\rangle$ and $\langle\sigma_{22}(t)\rangle$. The ionization probability at the end of the square pulse (constant intensity) at a time T would normally be given by $P_{ion}(T)=1-\langle\sigma_{11}(T)\rangle-\langle\sigma_{22}(T)\rangle$. However, at time T there will be population in the excited state that will decay to the continuum with a rate Γ due to the configuration interaction (the spontaneous decay rate is negligible compared to Γ). Therefore, in order to account for this population we should express the ionization probability at times $t>T$ as

We can now plot the ionization probability calculated at a time $t>T$ as a function of the driving frequency around the resonance, for various intensities, laser bandwidths and interaction times T.

However, in addition to the ionization of the neutral, the radiation can ionize the $He(1s)^+$ ions produced from autoionization. This process involves the absorption of one additional photon. If it is electrons or He ions that are counted, the resulting α-particles do not influence the observation. But in transmission, those additional photon absorptions do contribute to the counting. The calculation must therefore include that additional channel of photon absorption, for which the cross section is $1.2\times10^{-18}cm^2$; about the same as the one for the single-photon ionization of the neutral, at the smooth part of the continuum away from the resonance. For the sake of completeness, we have included that additional channel in our calculations, by writing

$$\dot{P}^{\diamondsuit}_{ion}(t)=\dot{P}_{ion}(t)-P^{\diamondsuit}_{ion}(t)\gamma_{DI} \tag{4.17}$$

where $P^{\diamondsuit}_{ion}(t)$ is the ionization probability including the double ionization of Helium and γ_{DI} is double ionization rate which is the product of the double ionization cross section and the flux.

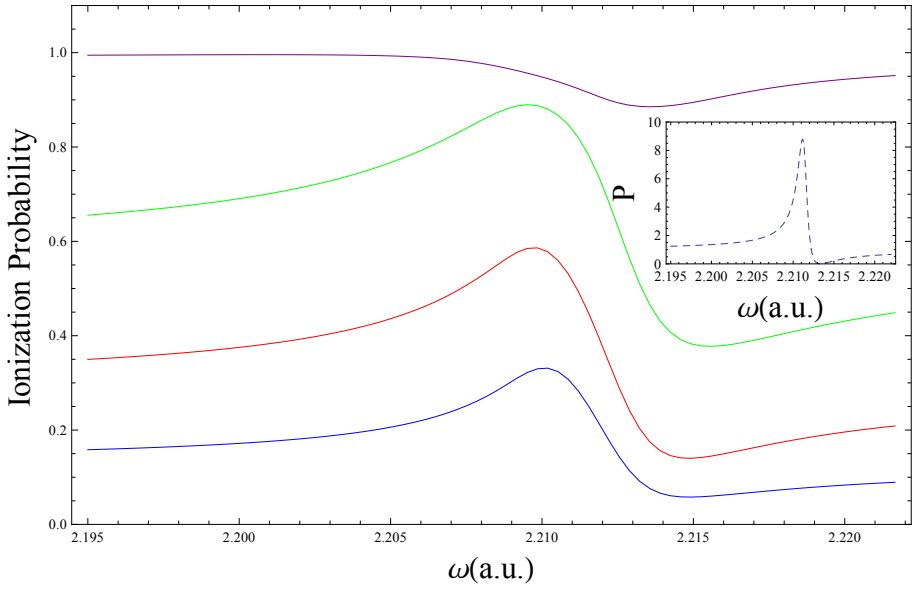

FIGURE 4.1: Probability of ionization as a function of the driving frequency for various intensities with pulse duration $T = 50fs$ and laser bandwidth $\gamma_L = 0.0018a.u.$ Blue Line: $I_0 = 2\times10^{13}W/cm^2$, Red Line: $I_0 = 5\times10^{13}W/cm^2$, Green Line: $I_0 = 10^{14}W/cm^2$ and Purple Line: $I_0 = 5\times10^{14}W/cm^2$. In the inset, we show the standard Fano profile for $q = -2.75$.

For Helium 2s2p $^1P^0$ AIS, the parameters involved in the theory (expressed in atomic units) are

$$q = -2.75 \qquad \Gamma = 1.37\times10^{-3} \qquad \Omega = 0.025\frac{E_0}{2} \qquad \gamma = 0.1775\mathrm{I}_0$$

For every system, the above four parameters are related through the equation $4\Omega^2 = q^2\gamma\Gamma$. The values of these parameters must be obtained through an elaborate atomic structure calculation, which has been done in numerous papers [23–25]. Note that in the Rotating Wave Approximation (RWA), the relation between the intensity and our definition of the electric field is $I = \frac{1}{2}\mathcal{E}(t)^2$. Clearly Ω^2 and γ are proportional to the radiation intensity, which cancels out in the equation that constrains the four parameters.

We also set $\omega_g = 0$, therefore the energy difference ω_{ag} ($\hbar = 1$) is equal to the energy of the 2s2p $^1P^0$ AIS, namely $\omega_{ag} = 65.40eV \simeq 2.211a.u.$ The autoionization lifetime is approximately 18fs.

We begin by considering an example with conditions typical to FEL-FLASH radiation. In addition to the atomic parameters given above, we need values for the peak intensity, the pulse duration and the laser bandwidth. Adopting, for the purposes of this quantitative illustration, values typical to experiments at FLASH, we obtain the results depicted in Fig.4.1. None of the four profiles, even the one for the lowest intensity, resembles the usual textbook profile $P = (q+\varepsilon)^2/(1+\varepsilon^2)$, which is shown in the inset of Fig.4.1. An attempt to fit even the lowest intensity (blue) curve with the standard parameters q and ε, would lead to a totally irrelevant value of q.

A brief parenthesis is in order at this point. Since for experimental reasons, instead of the ion or electron profile, often it is the photon transmission spectrum in terms of Beer's law that is measured, in Fig.4.2 we show the transmission spectra

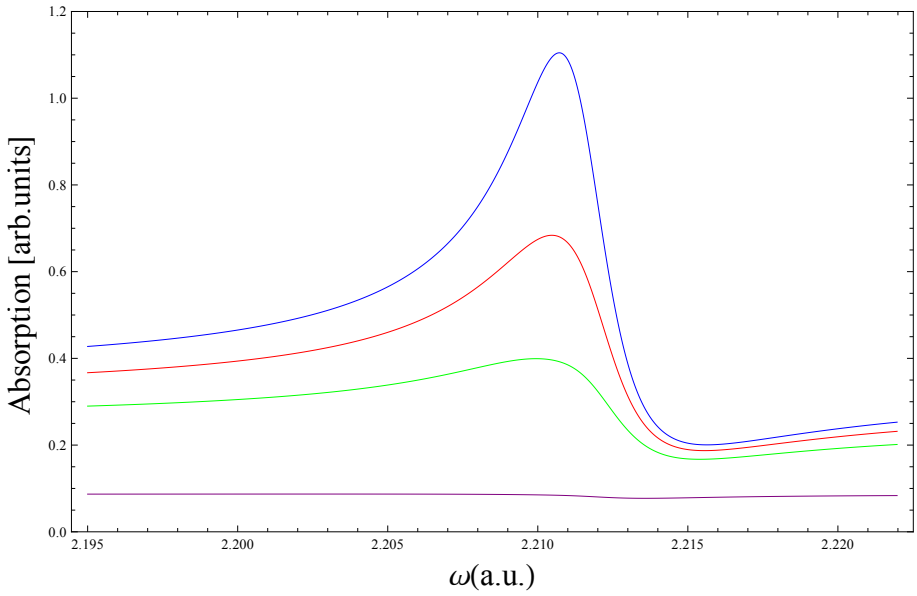

FIGURE 4.2: Absorption Spectrum as a function of the driving frequency for various intensities with pulse duration $T = 50fs$ and laser bandwidth $\gamma_L = 0.0018a.u.$ Blue Line: $I_0 = 2\times10^{13}W/cm^2$, Red Line: $I_0 = 5\times10^{13}W/cm^2$, Green Line: $I_0 = 10^{14}W/cm^2$ and Purple Line: $I_0 = 5\times10^{14}W/cm^2$.

corresponding to the parameters of Fig.4.1 for typical values of interaction length and number density of the medium. The observed signal is now seen to decrease with increasing intensity, simply because in Beer's law the transmission through the medium is divided by the incoming radiation. Nevertheless, there is a one to one correspondence between ion (electron) signal and transmission. The distortion of the profile is obvious in both observations. Having settled the equivalence between ion and transmission signals, we will hereafter confine our discussion to ion spectra.

From half a century or so of laser spectroscopy, we know that driving a resonant transition strongly, we should expect a distortion of the excitation profile. For bound-bound transitions, with negligible Doppler and collisional broadening, strong driving implies a Rabi frequency larger than the dominant relaxation rate [2, 3]. Since for bound-bound transitions the profile tends to be Lorentzian, typically the relaxation is reflected in the width at half maximum of the profile. Even in the context of XUV or shorter wavelength radiation, where Auger decay may be the dominant relaxation, the profile is Lorentzian [20]. In autoionization with a relatively small q parameter, however, the AI width Γ does not correspond to the width of the AI at half maximum. Even the notion of half maximum is not obvious in that case. Let us, nevertheless, agree here to define the maximum, in relation to the background for large ε, which, in the inset of Fig.4.1, leads to a value for P equal to one. Sidestepping straightforward mathematical details here, let us note that for the case of He(2s2p) with $q = -2.75$, the width Γ of the profile is to be found slightly above the half maximum, in the sense defined above.

For Lorentzian profiles, strong driving usually leads to what is referred to as power broadening, which means that the profile tends to become "fatter" [26]. In the limit of Rabi frequency much larger then the relaxation constant, we have an AC Stark splitting, which is observable if one of the resonant (usually the upper) states,

is probed by a weak transition to another state. As we showed in previous sections, these issues have been formulated and discussed rather extensively even for AI states. The effect of field fluctuations, including intensity fluctuations, for strong coupling in bound-bound transitions, has been studied in exhaustive detail [2, 3], but not in the case of AI resonances; simply because sources for the strong driving in the XUV and beyond did not exist, until the recent advent of the short wavelength FEL. A step in that direction has been reported in [20], in which the behavior of an Auger resonance driven strongly by a field with intensity fluctuations, such as those of the FEL, has been studied in great detail. To the best of our knowledge, strong driving of an AI state, such as the He(2s2p), under FEL radiation has not been observed, but this is probably a matter of short time. And the theory of an asymmetric AI state driven strongly by a field with intensity fluctuations, such as that of current FEL's turns out to be quite challenging.

Returning now to the case of driving below the strong Rabi boarder-line, we have already shown unexpected distortion of the profile, as documented by the three lowest intensity curves in Fig.4.1. We can safely rule out any visible contribution from power broadening. However, although the intensity may be below the strong field, the amount of ionization by the end of the pulse can still be substantial. The point to be stressed, in this connection, is that for a pulsed source of significant intensity, pulse duration and peak intensity cannot be viewed independently. For example, a pulse of 50 fs duration may sound short and a peak intensity of $10^{14}W/cm^2$ may be below the strong coupling value. Put the two together, and substantial ionization occurs, which means that for that intensity, a pulse of 50 fs duration is a long pulse. In a time dependent situation, such as the one embodied in the density matrix equations, the amount of ionization is not simply proportional to time, as in Fermi's golden rule. As a result the ionization on resonance increases differently than it does in the wings of the profile; hence the profile distortion. One might conjecture that the distortion due to pulse duration would be minimized, or even eliminated, by decreasing the pulse duration. However, the Fourier bandwidth is lurking in that process and eventually distortion due to the increased Fourier bandwidth, inherently included in the time-dependent calculation, begins setting in. Lest the reader be concerned with the particular temporal shape of the pulse, which has been a Gaussian in our calculations, long experience with similar calculations, including those in the present context, has shown that such details have minimal quantitative effect on the main features of the problem.

The reader may have noticed that one of the curves in Figs.4.1 and 4.2 has been obtained with an intensity larger, by a factor of 2.5, than the strong coupling limit, in which case the DA has began to lose its validity. From related calculations for an Auger resonance [20], we know that the error is not sufficiently large to alter the main features. A qualitative argument drawn for the case of bound transitions, can be fairly convincing here. Since the Rabi frequency is proportional to the field, a factor of 2.5 in intensity, entails a factor of about 1.58 increase in the Rabi frequency. This would imply a factor of about 1.58 in the apparent width of the resonance. Yet the profile for that intensity, bears no resemblance whatsoever to a Fano resonance. Actually it looks like what is usually referred to as "window resonance", exhibiting only a shallow minimum; a rather dramatic illustration of the interplay between pulse duration and intensity, brought about by a mere factor of 2.5 of increase in intensity. Obviously the reason the minimum is not sharp has to do with the bandwidth of the source, as the wings of the radiation profile sample transition amplitude around the minimum.

One might temped to say that the distortion of the profile in high intensities is

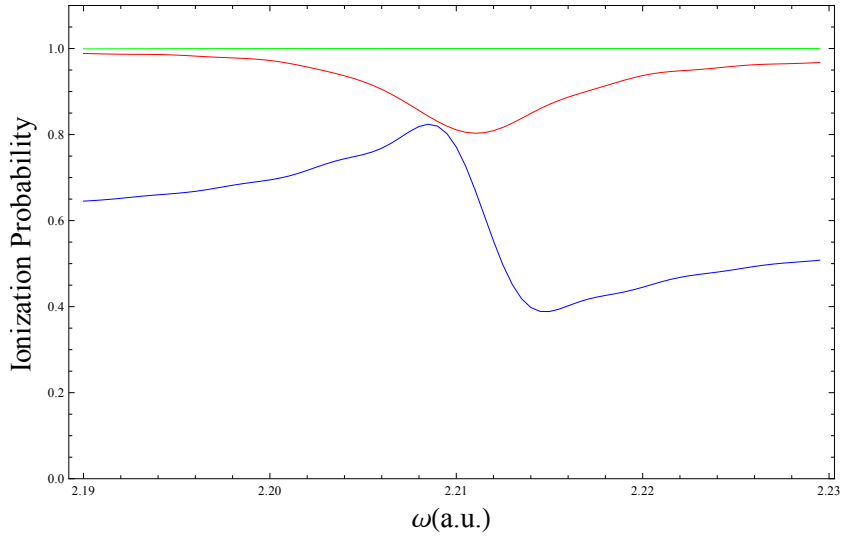

FIGURE 4.3: Probability of ionization as a function of the driving frequency for various intensities and $T = 25fs$, $\gamma_L = 0.0018a.u.$ Blue Line: $I_0 = 2 \times 10^{14} W/cm^2$, Red Line: $I_0 = 10^{15} W/cm^2$ and Green Line: $I_0 = 2 \times 10^{16} W/cm^2$.

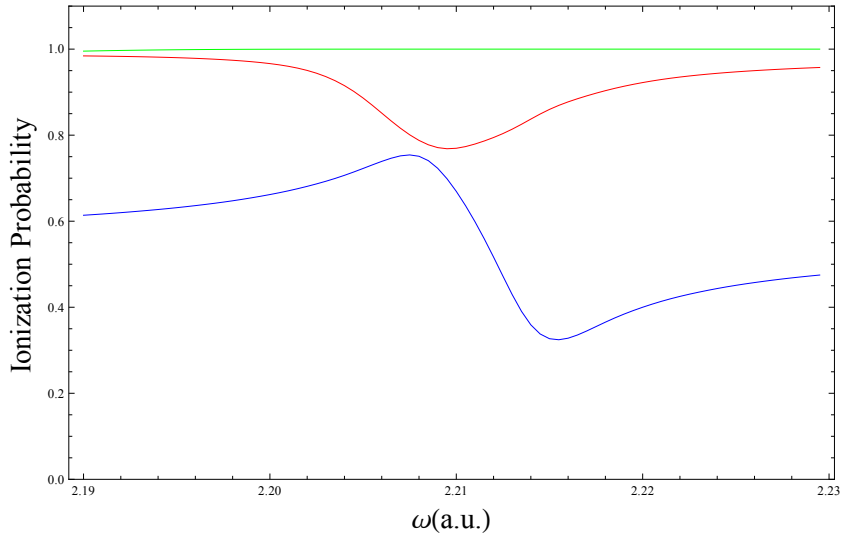

FIGURE 4.4: Probability of ionization as a function of the driving frequency for various intensities and $T = 25fs$, $\gamma_L = 0.0018a.u.$ under a Gaussian pulse. Blue Line: $I_0 = 2 \times 10^{14} W/cm^2$, Red Line: $I_0 = 10^{15} W/cm^2$ and Green Line: $I_0 = 2 \times 10^{16} W/cm^2$. For a Gaussian pulse we refer to I_0 as the peak intensity.

due to the power broadening. Although the intensity plays a significant role in the modifications of the AI profile, it is the combination of intensity and interaction time that truly determines whether the signal will be asymmetric or flat. In figure 4.3, we choose a smaller interaction time , i.e. $T = 20fs$ and intensities from moderate to high. At intensities such that the Rabi frequency is comparable to the AI width, we can see that the profile is not flat if the interaction time is chosen so that it is comparable to the AI lifetime. For such interaction times we can also see the appearance of some undulations, which are also evident in presence of a mid-to-strong

non-fluctuating field [4]. The source of such undulations is the Rabi cycling between the ground and the AI state, arising under proper combinations of interaction time and intensities. For very high intensities $I_0 \approx 10^{16} W/cm^2$, even for small interaction times, the profile is completely flat.

In order to have a quantitative comparison between the effect of the pulse shape to the AI profile, we use equations (4.15) and (4.16) to calculate the ionization probability for a Gaussian pulse using the parameters denoted in figure 2.

The comparison between figures 2 and 3 reveal that shape of the pulse plays practically no role on the determination of the AI profile, a result that is generally known and used for both analytical and numerical simplifications. The disappearance of the undulations in figure 3 is due to the fact that equations (4.15) and (4.16) are rate equations. For moderate to strong fields (see Blue and Red Line) rate equations do not account for the Rabi cycling that takes place between the ground and the AI state, resulting a smooth profile. Every figure has been tested with various types of pulses like square, Gaussian, Lorentzian, trapezoidal etc. and the results were for all practical purposes the same. However the use of a pulse of constant intensity is a root for analytical solutions resulting efficiency in calculations. Therefore for sake of simplicity, we will present our results here using constant intensities and use Appendix A to present the same results using Gaussian pulses, in order to have a quantitative comparison for various parameters. Comparison of figures 2 and 3 also reveals that equations (4.15) and (4.16) provide results in very good agreement with the exact results using a constant intensity, even for intensities such that the Rabi frequency becomes comparable to the AI lifetime where the approximation (4.14) tends to become questionable.

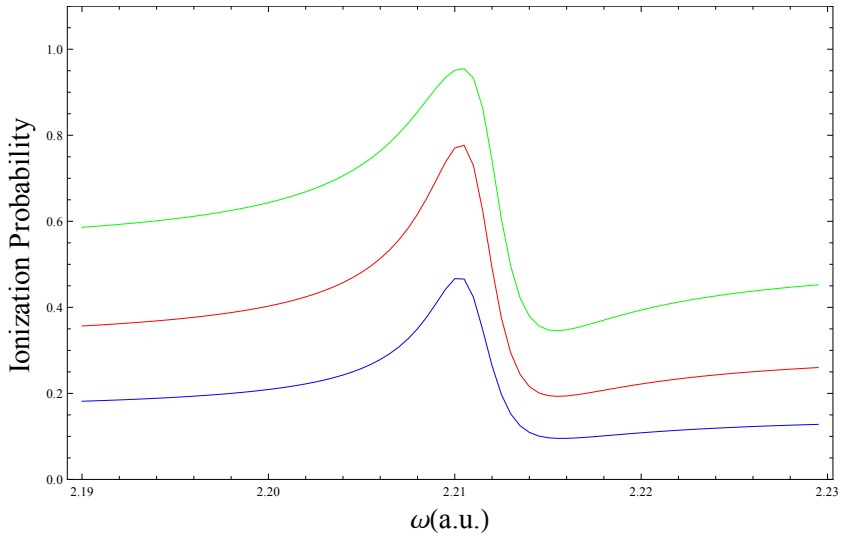

FIGURE 4.5: Probability of ionization as a function of the driving frequency for various interaction times T and $I_0 = 10^{13} W/cm^2$, $\gamma_L = 0.0018 a.u.$ Blue Line: $T = 100 fs$, Red Line: $T = 240 fs$ and Green Line: $T = 480 fs$.

In figure 4.5 we explore the effects of the interaction time on the AI profile for a weak field of constant intensity. As the interaction time increases, the ionization probability generally increases, as the atom has more time available to get ionized. The interaction times were chosen such that they are larger than the AI lifetime. The general picture arising from figures 4.1 to 4.5 is that the ionization is mainly

determined from whether the system is time saturated, i.e. if for a given intensity the time that the field is present is sufficiently enough for the atom to get ionized.

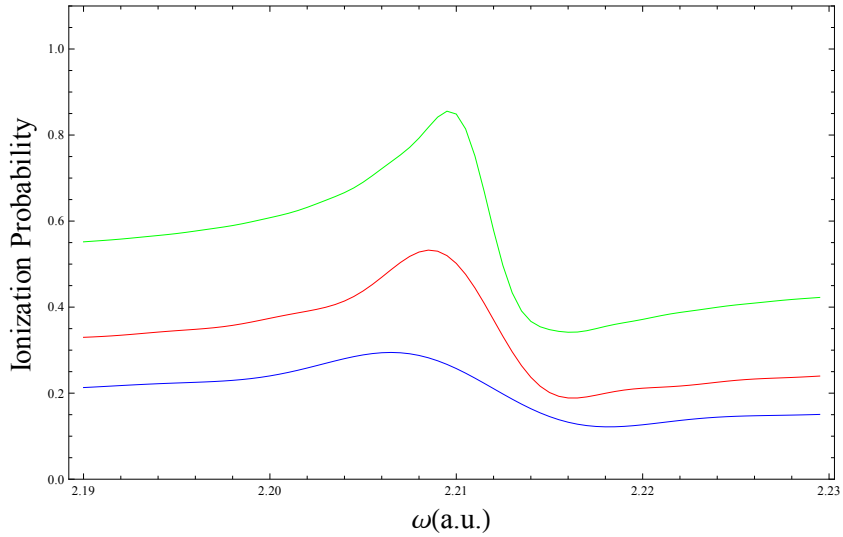

FIGURE 4.6: Probability of ionization as a function of the driving frequency for various interaction times T and $I_0 = 10^{14} W/cm^2$, $\gamma_L = 0.0018 a.u.$ Blue Line: $T = 5fs$, Red Line: $T = 10fs$ and Green Line: $T = 20fs$.

However, if the pulse durations (interaction times) become sufficiently small (always relevant to the AIS lifetime and the coherence time), then we begin to observe a broadening of the profile and the asymmetry tends to be less clear. In figure 4.6 the interaction times are chosen such that they result a visible Fourier broadening. The main reason of this distortion is not the Fourier broadening itself, but a combination of power broadening and Fourier broadening due to short pulse durations, with the last being the dominant broadening mechanism.

If we set the laser bandwidth equal to zero, then as discussed in chapter 3.2 the phase-diffusion model represents a coherent field. In view of equation (3.16) we can use an average over the intensity distribution of the chaotic field to obtain an expression of the ionization probability for the chaotic field model with zero bandwidth (implying coherence times sufficiently larger than the AI lifetime). In figure 4.7 we compare the efficiency on ionization between a coherent and a chaotic field, using typical parameters from the weak to the strong field limit. As we can clearly see, in all intensity regimes the chaotic field is less effective on ionization than a coherent field. This efficiency is enhanced when we tune the driving frequency in the vicinity of the resonant frequency ω_{21}.

We generally could expect no enhancement of the probability using a chaotic field since the process is linear. It has been generally shown [27–29] that in the weak field limit far from resonance there is an enhancement of about N! for a N-photon process using a chaotic field instead of a coherent. Since our process involves the absorption of 1-photon, in this regime we expect no enhancement of the process and this is indeed reflected in the blue curves of figure 4.7 where in the off-resonance limit they have the same behaviour. However, if the frequency is resonant with the transition $|1\rangle \leftrightarrow |2\rangle$ and/or if the intensity is large enough, this picture can change drastically. In fact this issue was studied recently in exclusive detail for multi-photon processes in my undergraduate thesis and the results showed that this enhancement

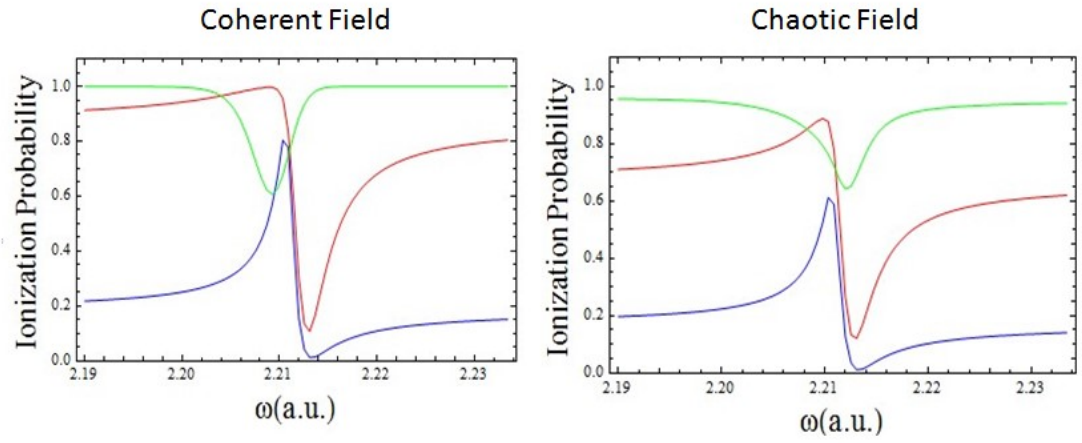

FIGURE 4.7: Comparison between the probability of ionization in presence of a coherent and a chaotic field of zero bandwidth as a function of the driving frequency for various intensities and $T = 150fs$ Blue Line: $I_0 = 10^{13}W/cm^2$, Red Line: $I_0 = 10^{14}W/cm^2$ and Green Line: $I_0 = 10^{15}W/cm^2$.

is modified significantly on resonance. We have also shown that there are also regions where the enhancement can turn the other way around and the chaotic field which was N! times more efficient for weak fields, can become less efficient than a coherent field.

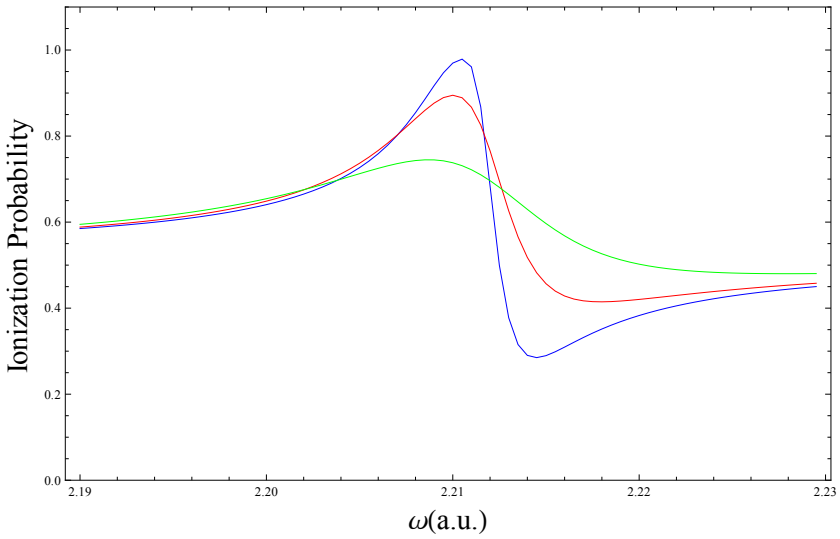

FIGURE 4.8: Probability of ionization as a function of the driving frequency for various laser bandwidths and $I_0 = 10^{13}W/cm^2$, $T = 240fs$. Blue Line: $\gamma_L = 0.00108a.u.$, Red Line: $\gamma_L = 0.0036a.u.$ and Green Line: $\gamma_L = 0.0108a.u.$

Finally, in figure 4.8 we study the effect of the field bandwidth on the AI profile. We can clearly see that when the bandwidth of the field becomes sufficiently larger than the autoionization width $\Gamma = 1.37 \times 10^{-3}a.u.$, the FWHM of the profile

is mainly determined by γ_L. As the bandwidth increases the curve spreads and both the minimum and the maximum tend to smooth out. For very large bandwidths the asymmetry tends to become less visible since the profile becomes almost flat. If the bandwidth is sufficiently smaller than the AI width then the FWHM is determined mainly by Γ or by the interaction time if in general is smaller than the AI lifetime. These effects were of no importance since all experiments were carried out using synchrotron sources which have small bandwidths. However, the theory shows that when the laser bandwidth is included in calculations, the resulting profiles can be distorted dramatically under certain combinations of the relevant parameters. Therefore, the interpretation of modern AI experiments using FEL sources has to necessarily be accompanied with a theory that accounts properly for the stochastic properties of such sources.

The picture emerging from the above results should now be clear. The excitation of an AI resonance by a pulsed source, of intensity even below the strong coupling limit, will exhibit a profile that depends on the combination of the source parameters. Under such conditions, one cannot expect to observe the textbook Fano profile. We have, moreover, demonstrated extreme sensitivity to the combination of source parameters. After all, an uncertainty of a factor of 2 in the peak intensity delivered by an FEL is not that exorbitant. The positive side of our findings is that the modified AI profile can serve as a probe of the source parameters. That is because in our calculations, we have found that a particular profile is rather sensitive to the combination of parameters compatible with its shape. For example, one may have to decide which of the three main parameters, be it peak intensity, bandwidth, pulse duration, is/are known with higher accuracy, so as to extract the value of one or two of the others.

Appendix A

Gaussian pulse shape results

In this appendix we will present our results using the same parameters as those used in some of the figures of section 4.2 but using Gaussian pulse shapes. These results are crucial since they will indicate whether the shape of the pulse leads to significant changes to the AI profile.

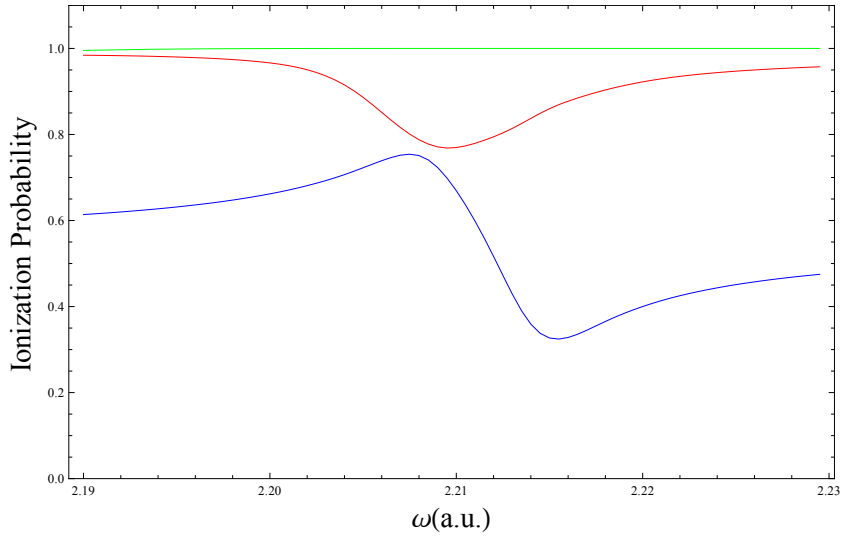

FIGURE A.1: Probability of ionization as a function of the driving frequency for various intensities and $T = 25fs$, $\gamma_L = 0.0018a.u.$ under a Gaussian pulse. Blue Line: $I_0 = 2 \times 10^{14} W/cm^2$, Red Line: $I_0 = 10^{15} W/cm^2$ and Green Line: $I_0 = 2 \times 10^{16} W/cm^2$. For a Gaussian pulse we refer to I_0 as the peak intensity.

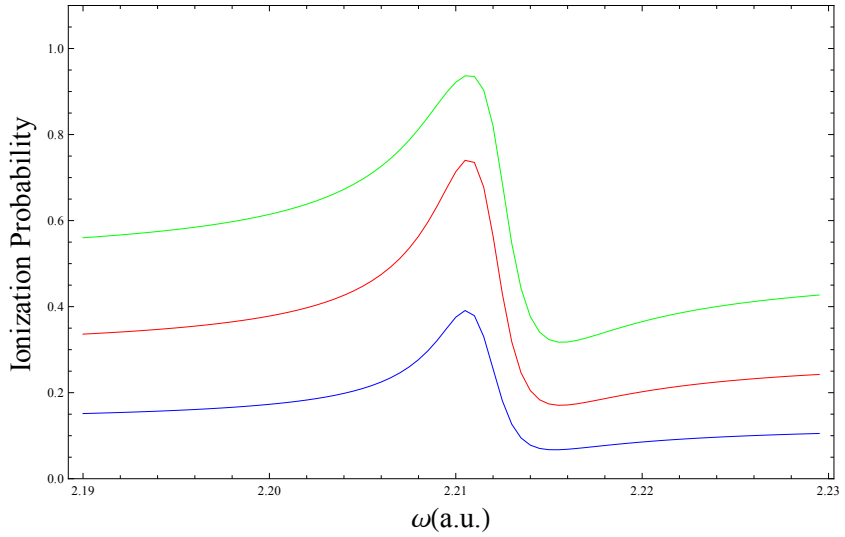

FIGURE A.2: Probability of ionization as a function of the driving frequency for various interaction times T and $I_0 = 10^{13} W/cm^2$, $\gamma_L = 0.0018 a.u.$ under a Gaussian pulse. Blue Line: $T = 100 fs$, Red Line: $T = 240 fs$ and Green Line: $T = 480 fs$. For a Gaussian pulse we refer to I_0 as the peak intensity.

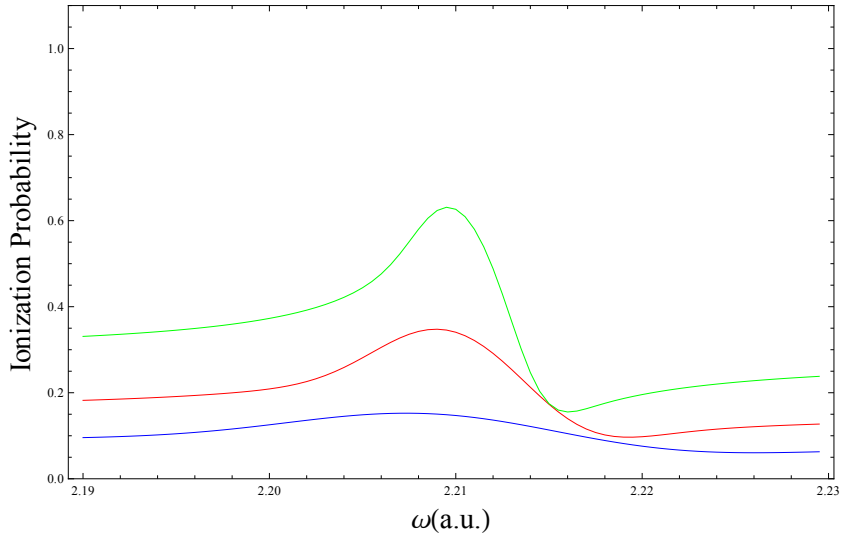

FIGURE A.3: Probability of ionization as a function of the driving frequency for various interaction times T and $I_0 = 10^{14} W/cm^2$, $\gamma_L = 0.0018 a.u.$ under a Gaussian pulse. Blue Line: $T = 5 fs$, Red Line: $T = 10 fs$ and Green Line: $T = 20 fs$. For a Gaussian pulse we refer to I_0 as the peak intensity.

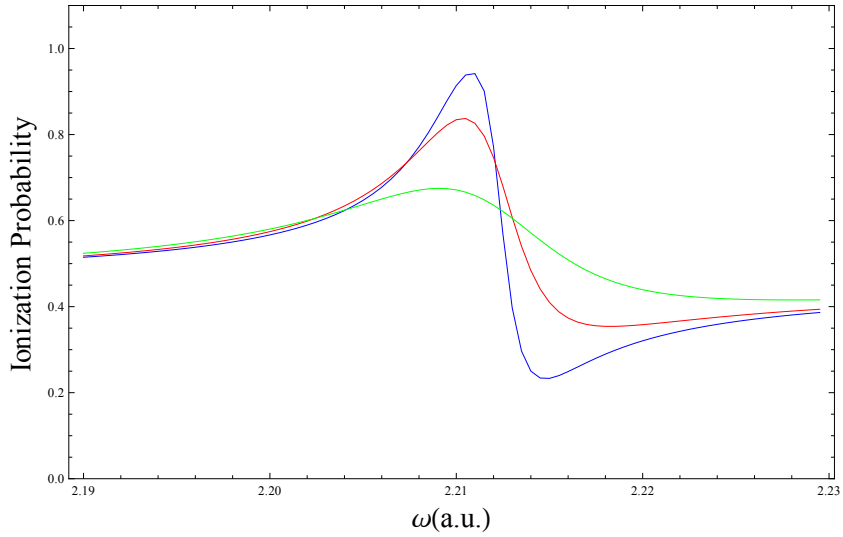

FIGURE A.4: Probability of ionization as a function of the driving frequency for various laser bandwidths and $I_0 = 10^{13} W/cm^2$, $T = 240 fs$ under a Gaussian pulse. Blue Line: $\gamma_L = 0.00108 a.u.$, Red Line: $\gamma_L = 0.0036 a.u.$ and Green Line: $\gamma_L = 0.0108 a.u.$ For a Gaussian pulse we refer to I_0 as the peak intensity.

Comparing the above the diagrams with the ones presented in chapter 4.2 we can safely assume that the shape of the pulse generally plays no important role on the determination of the AI profile. This result is generally known and is widely used for analytical and numerical simplifications. However, the comparison between figure 4.6 and A.3 reveals the if the pulse durations are of the order of the AI lifetime, the Gaussian pulse is less effective on ionization than a square pulse. This seems quite logical since the square pulse forces the atom to be driven by a field whose intensity is I_0 over the whole duration of the pulse, whereas the Gaussian pulse has a peak value of I_0 and its wings at smaller intensities. The above results have also been tested with trapezoidal and Lorentzian pulse shapes and the picture doesn't differ a lot, therefore their presentation here is not that important.

Bibliography

[1] E.Arimondo, Charles W.Clark and W.C Martin, Rev.Mod.Phys. **82**, 1947 (2010)

[2] A.T.Georges, P.Lambropoulos, Phys.Rev.A **20**, 991 (1979)

[3] A.T.Georges, P.Lambropoulos and P.Zoller, Phys.Rev.Lett. **42**, 1609 (1979)

[4] P.Lambropoulos and P.Zoller, Phys.Rev. A **24**, 379 (1981)

[5] S.I.Themelis, P.Lambropoulos and M.Meyer, J.Phys.B **37**, (2004)

[6] L.B.Madsen and P.Lambropoulos, J.Phys. B **34**, 1855 (2000)

[7] L.B.Madsen, P.Schlagheck and P.Lambropoulos, Phys.Rev. A **62** 622719 (2000)

[8] L.B.Madsen, P.Schlagheck and P.Lambropoulos, Phys.Rev.Lett. **85**, 42 (2000)

[9] N.E.Karapanagioti, D.Charalambidis, C.J.Uiterwaal, C.Fotakis, H.Bachau, I.Sanchez and E.Cormier, Phys.Rev. A **53**, 2587 (1996)

[10] Zhi-Heng Loh, Chris H. Greene and Stephen R. Leone, Chem.Phys. **350**, 7 (2007)

[11] P.Lambropoulos, Appl.Opt. **19**, 3926 (1980)

[12] U.Fano, Nuovo Cimento **12**, 154 (1935)

[13] U.Fano, Phys.Rev. **124**, 1866 (1961)

[14] Takashi Nakajima and P.Lambropoulos, Phys.Rev. A **50**, 595 (1992)

[15] Takashi Nakajima and P.Lambropoulos, Phys.Rev.Lett. **70**, 1081 (1993)

[16] L.A.A.Nikolopoulos, Takashi Nakajima and P.Lambropoulos, Eur.Phys.J.D **20**, 297-304 (2002)

[17] P.A.Apanasevich, G.I.Zhovna and A.P.Khapalyuk, J.Appl.Spectrosc. **8**, 14 (1968)

[18] A. Papoulis, *Probability, Random Variables and Stochastic Processes* (McGraw-Hill), New York (1965)

[19] J.R.Klauder and E.C.Sudarshan, *Fundamentals of Quantum Optics* (Benjamin) New York, (1968)

[20] G.M.Nikolopoulos and P.Lambropoulos, Phys. Rev. A **86**, 033420 (2012); J. Phys.B **46**, 16 (2013)

[21] S.G.Przhibelskii, Opt.Spectrosc. **42**, 8 (1977)

[22] P.Elyutin, Opt.Spectrosc. **43**, 318 (1977)

[23] E.Lindroth, Phys.Rev. A **49**, 4473 (1994)

[24] T.N.Rescigno, C.W.Jr.McCurdy and A.E. Orel, Phys.Rev. A **17**, 1931 (1978)

[25] Froese Fischer C, Comput.Phys.Commun. **128**, 635 (2000)

[26] M.L.Citron, H.R.Gray, C.W.Gabel and C.R.Stroud, Jr.Phys. Rev. A **16**,1507 (1977)

[27] B.R.Mollow, Phys.Rev. **175**, 1555 (1968)

[28] G.S.Agrawal, Phys.Rev. A **1**, 1445 (1970)

[29] P.Lambropoulos, Advan.At.Mol.Phys. **12**, 87-163 (1976)